Wake Mixing Control For Floating Wind Farms

Analysis of the Implementation of the Helix Wake Mixing Strategy on the IEA 15-MW Floating Wind Turbine

van den Berg, D.G.; De Tavernier, Delphine; Marten, David; Saverin, Joseph; Van Wingerden, Jan Willem

DOI
10.1109/MCS.2024.3432341

Publication date
2024

Document Version
Final published version

Published in
IEEE Control Systems

Citation (APA)
van den Berg, D. G., De Tavernier, D., Marten, D., Saverin, J., & Van Wingerden, J. W. (2024). Wake Mixing Control For Floating Wind Farms: Analysis of the Implementation of the Helix Wake Mixing Strategy on the IEA 15-MW Floating Wind Turbine. *IEEE Control Systems*, *44*(5), 81-105. https://doi.org/10.1109/MCS.2024.3432341

Wake Mixing Control For Floating Wind Farms

ANALYSIS OF THE IMPLEMENTATION OF THE HELIX WAKE MIXING STRATEGY ON THE IEA 15-MW FLOATING WIND TURBINE

DANIEL VAN DEN BERG, DELPHINE DE TAVERNIER, DAVID MARTEN, JOSEPH SAVERIN, and JAN-WILLEM VAN WINGERDEN

Digital Object Identifier 10.1109/MCS.2024.3432341
Date of current version: 6 September 2024

Achieving the European Union's target of 510 GW of installed wind energy capacity by 2030 requires a significant expansion of the currently installed capacity of 255 GW [1], [2]. As a consequence of these ambitions, the power density of newly developed wind farms is rising by increasing the number of turbines within a wind farm and the size of individual turbines [3]. The larger wind farms are predominantly located offshore where wind conditions are more consistent and, on average, wind speeds are higher compared to onshore locations [4]. Furthermore, more than 80% of Europe's wind energy resources can be found in waters too deep for bottom-fixed turbines [5], [6], resulting in a sharp

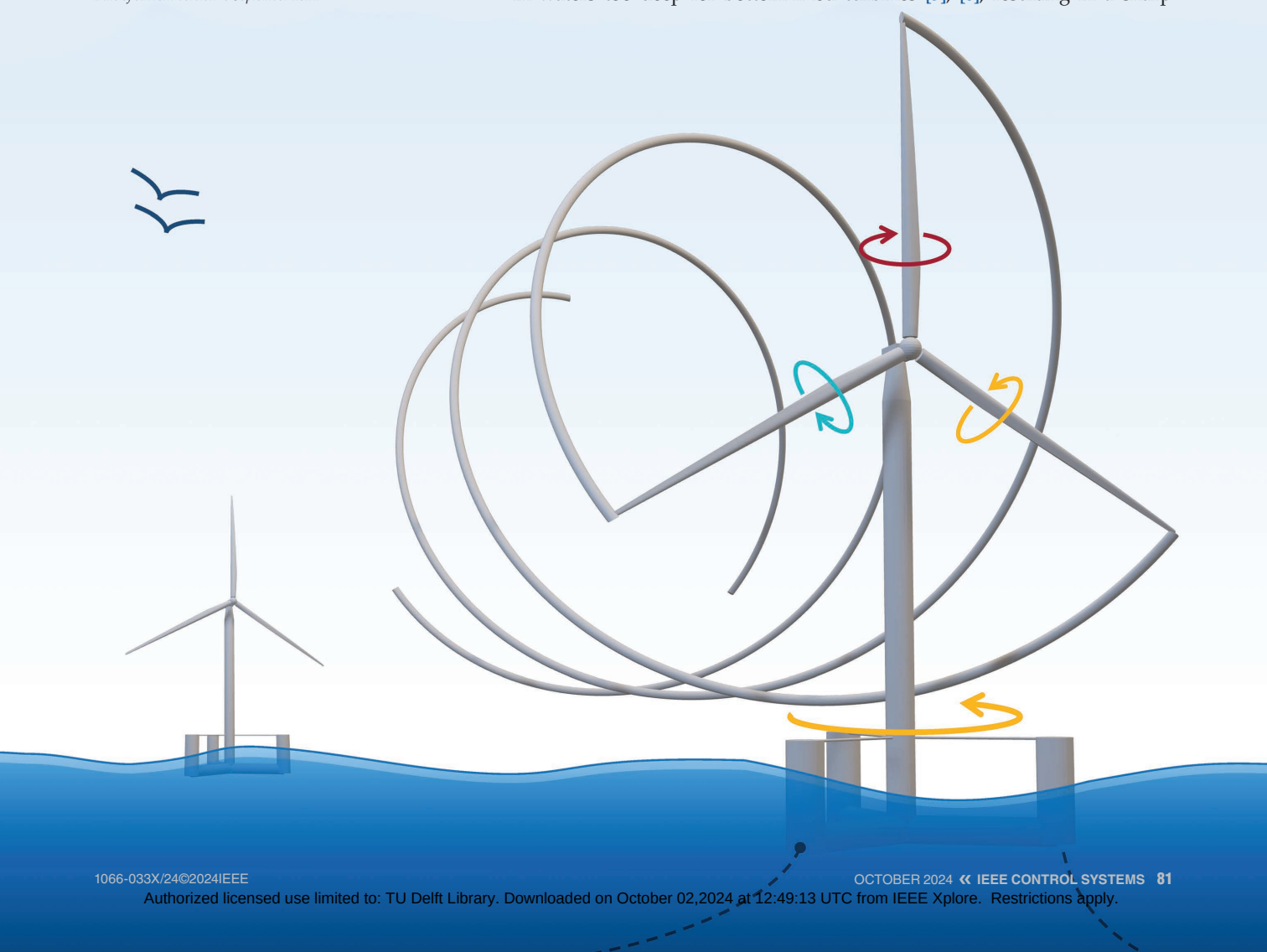

Summary

The ever-increasing demand for green energy production has led to an explosive growth in wind turbine technology, all in the interest of extracting as much energy from the airflow for a given plot of land. Floating wind turbines are less restricted by the limitations of offshore bottom-fixed turbines when it comes to the water depths at which they can be deployed. As such, they can be placed farther out at sea where wind speeds are more consistently higher.

The energy production of a wind farm can also be increased by reducing the wake interaction between turbines within the farm. In recent years, control solutions such as dynamic induction control (DIC) and dynamic individual pitch control (DIPC) have shown the potential to decrease this interaction by actively triggering the wake mixing process behind the turbine.

As floating wind technology matures, these wind farms will run into similar wake interaction challenges as their bottom-fixed counterparts. However, when transitioning wake control solutions from bottom-fixed turbines to floating turbines, they interact with the platform dynamics of these turbines. This coupling depends on the type of floater on which the turbine is mounted and results in the movement of the whole turbine. Typically, this movement is undesired, and extensive research has gone into the control of floating turbines with the aim of minimizing platform movement.

Recent work has also shown that these movements can be leveraged to increase wind farm efficiency. This work investigates the coupling between the Helix wake mixing method and the platform dynamics of the floating turbine for the International Energy Agency (IEA) 15-MW turbine mounted on the VolturnUS-S floater. More specifically, it investigates if movement is triggered when the Helix is applied and how any potential movement impacts the wake mixing dynamics.

For this floater type, the frequency range within which the Helix wake mixing method typically is applied encompasses an eigenfrequency in yaw. At this eigenfrequency, which coincidentally lies close to the ideal mixing frequency, a typical blade pitch of 4° amplitude results in yaw motion of up to 8°. When the wind speed behind the actuated turbine is analyzed for both a bottom-fixed turbine and a floating turbine, a reduction in wake recovery is seen for the floating turbine. Moreover, the impact on wake recovery is largest at the eigenfrequency in yaw for this particular floating turbine, and the ideal mixing frequency has shifted compared to the IEA 15-MW bottom-fixed turbine.

increase in the interest in floating wind turbines over the past decade (see "Summary").

As wind turbines extract energy from the incoming wind, they create an area of turbulent low-velocity airflow behind them, often referred to as the turbine's *wake*. The force that the turbine exerts on the flow also creates an area of low velocity in front of the turbine. This area is often referred to as the *induction zone* of the turbine as it induces a lower velocity in the free stream. An example of the wake effect of a turbine can be seen in Figure 1, where the wakes of the upstream turbines in the Horns Rev wind farm are visible due to specific atmospheric conditions at the time of photographing. As these wakes travel downstream, they interact with the turbines behind the upstream turbines.

FIGURE 1 A visualization of wind turbine wakes for the Horns Rev wind farm. Atmospheric conditions were such that water vapor condensed due to the pressure change behind the wind turbines resulting in visible wakes. (Source: Image courtesy of Vattenfall, distributed under the CC BY-ND 2.0 license.)

This interaction causes extensive losses in energy production for the waked turbines. Research indicates that this loss can amount to up to 25% of the energy production of an otherwise unwaked turbine [7], [8]. Since wake interaction accounts for a significant loss in a wind farm's efficiency, it has been an area of substantial research [9]. The first investigation into the wake interaction between turbines dates back to the 1980s, with work discussing wake steering [10] and work that aims to develop a fast analytical model of the wind turbine wake in 1983 [11]. This model, often referred to as the *Jensen model*, introduced in [11], formed the basis of the development of many subsequent wake models, each further expanding upon their capabilities; see, for example, [12].

With the introduction of fast analytical wake models, the first major attempt at increasing the wind farm's efficiency was using wind farm layout optimization. Early work by [13] explored an optimization trading off power production and installation costs using the Jensen wake model to model turbine interaction. In more recent work [14], an increase in a wind farm's power production by 1–2% is realized by optimizing two existing wind farms using different wake modeling techniques. Current research focuses mainly on comparing optimization algorithms [15], [16], [17] or considers more complex onshore terrain complicating the optimization [18]. These optimizations typically assume the turbines to be static and aligned with the incoming wind direction. In

this scenario, the layout is designed such that power production is maximized for the prevailing wind direction, with diminishing gains for the remaining wind directions.

These diminished gains can be recovered by using a wake steering controller. Although the concept of wake steering was first introduced in [10] in 1982, it was discussed only within a purely academic framework. In 2001 [19] and 2005 [20], it was again covered, but the method significantly gained traction in both the scientific and industrial settings [21] in the past two decades. With wake steering, the turbine's nacelle is yawed to divert the wake away from any downstream turbine, increasing overall farm power production [22], [23], [24], [25], [26], [27].

As discussed in the aforementioned work, wake steering is an example of steady-state optimal control that is used to increase wind farm power production. Using engineering wake models, like FLORIS [28], lookup tables can be generated for ideal yaw angles for each turbine in a wind farm at given wind directions. Once yawed, the turbine's orientation is kept constant until the environmental conditions change. Recently, attempts have been made to incorporate control techniques such as wake steering into the layout optimization problem [29], [30]. Another recent advance in these wake models is the inclusion of the dynamic behavior of the wind field [31], [32]. This enables active control of turbines during time-varying wind conditions.

DYNAMIC WAKE MIXING TECHNIQUES

Other forms of control of wind turbines involve wake mixing techniques. Wake mixing control solutions can be classified as control techniques that use existing (or potentially novel) actuators available on the wind turbine to excite aerodynamic instabilities in the wake. Contrary to wake steering control, the primary goal of wake mixing is to dissipate the wake by promoting the wake roll-up dynamics. When a wake starts to mix, it reenergizes itself with the outside flow, increasing downstream wind speeds. The first wake mixing technique was proposed by [33], and a similar idea was already patented in [34].

In [33], an optimal control solution was sought to increase the energy capture through the boundary layer of the wake. In that work, a conjugate-gradient optimization method was used to find an optimal coefficient of thrust for each turbine such that energy extraction of the wind farm was maximized. The adjoint optimization was run within a large-eddy simulation of a wind farm of aligned turbines. The optimal control input resulted in a time-varying coefficient of thrust and led to an increase of 6.0% energy extraction of the wind farm. Analyzing the wake dynamics showed that the driving factor behind this increase is that with this control method, the wind speed in the wake becomes time varying, which promotes the mixing process.

The results presented in [33] led to the development of two active blade pitching techniques that are capable of achieving similar results as described in that work. These are dynamic induction control (DIC or the Pulse) [35] and dynamic individual pitch control (DIPC or the Helix) [36], [37], with the latter also being patented [38]. Both techniques use the blade pitch angle to control the turbine's thrust to promote the onset of wake mixing behind the turbine. The Pulse method uses the collective blade pitch angle to create a time-varying thrust coefficient. The Helix method differs from the Pulse in that regard as, with the Helix method, each blade is controlled individually, creating a helical induction zone. Simulations carried out in [37] for an aligned two-turbine wind farm showed that the aggregate power of the farm can be increased by 4.6% using the Pulse method and by 7.5% using the Helix method. For this investigation, the turbines are spaced at a distance of five rotor diameters apart. An example of the wakes of turbines actuated with the Pulse and Helix wake mixing methods is shown in Figure 2. Included in the figure is the wake of an unactuated turbine which often serves as a baseline comparison.

For novel techniques like the Pulse and the Helix, another area of research concerns the loading of the actuated turbine. The increase of downstream wind speed from wake mixing methods comes at the cost of increased loading of the upstream turbine [39], [40]. This needs to be taken into account when deciding to use these techniques on both bottom-fixed and floating turbines. Furthermore, when looking at the farm level, the turbines directly behind the actuated turbine will also see an increase in loading due to the increased wind speed they experience. For example, in [39], an increase of 8% in blade loads is reported for the second turbine when the Helix is activated on the upstream turbine.

THE TRANSITION TO FLOATING WIND

Within this work, we explore how dynamic wake mixing control interacts with floating wind turbines and if it can significantly reduce this wake interaction between turbines. In particular, we will consider if the extra six degrees of

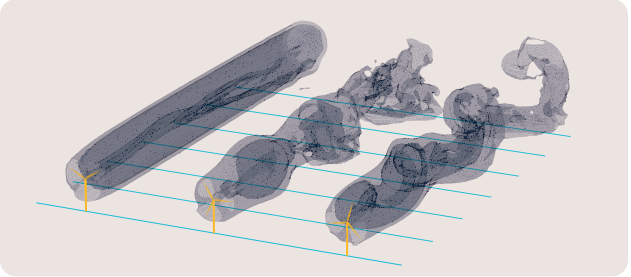

FIGURE 2 The wakes of three turbines each with different control targets. The domain is 1,500 m long with every blue line spaced by 250 m. The turbine on the left is set to what is called *greedy* control as it aims to extract the most amount of energy from the wake. This creates a long uniform wake of low wind speed, represented by the darker color. The middle turbine and the rightmost turbine use the Pulse and Helix, respectively. Notice how the wake for the Pulse expands and contracts over distance. This pulsating (hence 'The Pulse') effect promotes wake mixing. Both methods induce wake mixing, which disrupts the wake and increases downstream wind speed. (Source: Image generously created by Marcus Becker.)

freedom of a floating turbine can be leveraged to mitigate the wake interaction. These six degrees of freedom consist of three translational ones: surge, sway, and heave, and three rotational ones: roll, platform pitch, and yaw, which are defined in Figure 3. These extra degrees of freedom typically complicate the design of these kinds of turbines and controllers. However, from a control perspective, this also offers extra opportunities for mitigating the wake interaction between turbines. One such example is the ability to actively relocate the turbines within a floating wind farm to minimize the wake overlap [41], [42], [43]. This topic is also covered in the contribution in this edition of *IEEE Control Systems Magazine* by Niu et al. [85]. By altering the yaw angle and magnitude of the thrust vector, [42] increased the efficiency of an idealized wind farm by 5–10% by relocating the floating turbines. The exact gain depends on the wind direction for which the farm is being repositioned.

Alternatively, some of the mechanical properties of the floater can also be adapted during operation. For specific floaters, water can be pumped into the columns, altering the roll or platform pitch angle of the platform. Pitching the platform of a floating turbine has a similar effect on the wake as when the nacelle of a turbine is intentionally misaligned in yaw with the incoming flow. In both cases, the misalignment creates a force component perpendicular to the incoming flow that deflects the wake behind the turbine. The concept of pitching the floating platform is explored in [44], where a 5% increase in the cluster is realized when the floater of the upstream turbine is pitched forward by 20°. At this platform pitch angle, the turbine deflects the wake toward the sea, allowing higher energy flow to enter from above the wake and reach the downstream turbine.

When the aforementioned wake mixing techniques are applied to a floating turbine, the time-varying thrust will excite the six degrees of freedom. If and how this movement influences the effectiveness of the wake mixing technique depends on the coupling between the wake control method and floating turbine dynamics. For the Pulse and the Helix, this is explored in [45], [46], and [47]. Furthermore, using the motions of the turbine for the benefit of wake mixing is patented in [48].

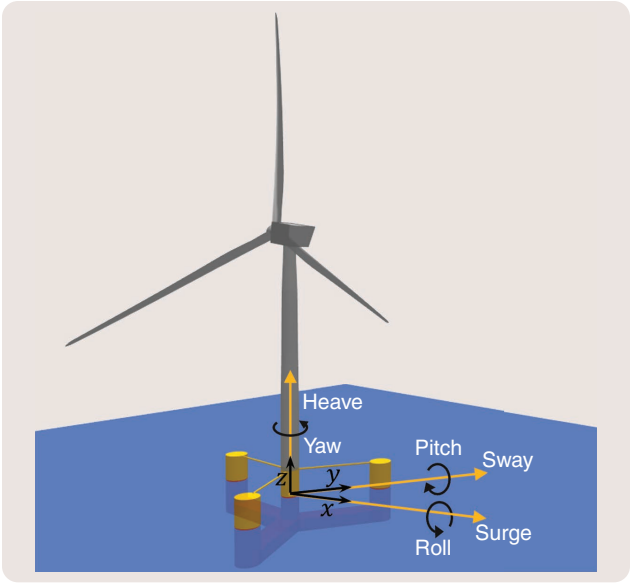

FIGURE 3 An axes system showing the six degrees of freedom for a floating turbine.

For the Pulse, the coupling was found to *reduce* the effectiveness of this particular wake mixing method. The work presented in [47] used prescribed motions to mimic the motions of a floating wind turbine. This approach, however, does not capture any further coupling between the platform motions and the mechanisms behind the Helix wake mixing technique.

This highlights one of the research gaps when transitioning controllers from bottom-fixed to floating turbines. Controllers optimized for bottom-fixed turbines might underperform when coupled to a floating turbine, or new optimal operating conditions need to be derived to account for the platform dynamics of the turbine.

RESEARCH OBJECTIVES

This work presents a comprehensive overview of the Helix wake mixing method and the coupling between aerodynamics and the structural- and hydrodynamics of a floating wind turbine. First, a frequency-domain analysis of the coupling between Helix and platform motions is presented, and second, time-domain simulations are executed to investigate the system using its full nonlinear representation. For these simulations, QBlade is used [49]. QBlade is a simulation suite capable of simulating hydro- and aero-elastics and wake dynamics.

THE DEVELOPMENT OF THE HELIX METHOD

This section will introduce the Helix wake mixing method. First, the Helix method's principle, derived from IPC for load mitigation and DIC, will be introduced. Second, an interpretation will be given of the Helix's effect on the wind turbine's thrust vector, and finally, how it induces wake mixing and its effect on the downstream wake. "Wake Mixing Background" provides a short aerodynamic background to the mixing process.

IPC

The Helix method was first proposed in [36] and further explored, for instance, in [37]. The main characteristic of the Helix is that it leverages the blade pitch degree of freedom of a wind turbine to manipulate the location of the point of origin of the resulting thrust vector. As a result of this dynamic thrust vector, the force exerted on the incoming flow will also be time varying, which, when excited at the right frequency, can lead to wake mixing increasing the power production of the downstream turbine. The inputs required to create the Helix are based on the same signals that are used for load mitigation using

IPC. It is, therefore, useful to consider the development of IPC and its (mainly mathematical) similarities to the Helix method.

IPC was developed with the goal of load mitigation [50], [51] and continues to be a topic of active research; see, for example, [40] and [52]. Typically, the dynamics and thus loads of a wind turbine are described in the rotating frame. The objective of an IPC controller is to minimize the fixed-frame loads to extend the lifetime of the turbine. The loads on the blades that are described in the rotating frame can be translated into the loads on the fixed turbine using the multiblade-coordinate transformation (MBC) [53].

The scheme of Figure 4 shows the general form of an IPC loop using the MBC. The blade root moments M_i, with $i \in [1, 2, 3]$, are transformed into the fixed-frame moments using the MBC transformation. Mathematically the MBC transformation can be expressed as

$$\begin{bmatrix} M_{\text{col}}(t) \\ M_{\text{tilt}}(t) \\ M_{\text{yaw}}(t) \end{bmatrix} = \frac{2}{3} \begin{bmatrix} 0.5 & 0.5 & 0.5 \\ \cos(\psi_1(t)) & \cos(\psi_2(t)) & \cos(\psi_3(t)) \\ \sin(\psi_1(t)) & \sin(\psi_2(t)) & \sin(\psi_3(t)) \end{bmatrix} \begin{bmatrix} M_{y,1}(t) \\ M_{y,2}(t) \\ M_{y,3}(t) \end{bmatrix} \quad (1)$$

in which M_{col}, M_{tilt}, and M_{yaw} are the fixed-frame moments and ψ_i is the azimuth angles of the individual blades with $i \in [1,2,3]$. The subscript col in M_{col} refers to the *collective* moment, that is, the moment on the entire rotor rather than the tilt or yaw axis. The transformation from individual blade pitch angles to fixed-frame blade pitch angles is synonymous to (1). The controller will output fixed-frame blade pitch angles, which can be transformed back to individual blade pitch angles using

$$\begin{bmatrix} \beta_1(t) \\ \beta_2(t) \\ \beta_3(t) \end{bmatrix} = \begin{bmatrix} 1 & \cos(\psi_1(t)) & \sin(\psi_1(t)) \\ 1 & \cos(\psi_2(t)) & \sin(\psi_2(t)) \\ 1 & \cos(\psi_3(t)) & \sin(\psi_3(t)) \end{bmatrix} \begin{bmatrix} \beta_{\text{col}}(t) \\ \beta_{\text{tilt}}(t) \\ \beta_{\text{yaw}}(t) \end{bmatrix} \quad (2)$$

which is known as the *inverse MBC transform*.

FROM IPC TO THE HELIX

While the main goal for IPC is to minimize the time-varying tilt and yaw moments (M_{tilt} and M_{yaw}), with the Helix method, a time-varying tilt and yaw moment is applied to the turbine. This is achieved by applying, in an open loop, a time-varying signal to the fixed-frame tilt (β_{tilt}) and yaw (β_{yaw}) pitch angle. A schematic representation of the open loop is given in Figure 5.

The type of signal used as an input in the fixed frame can be chosen freely. For this work, the inputs derived in

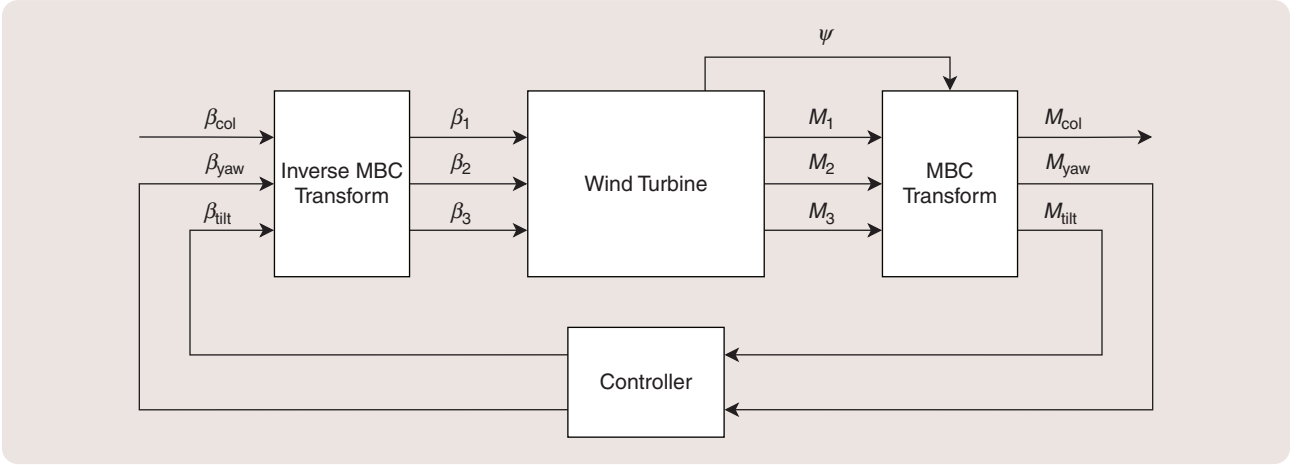

FIGURE 4 A general closed-loop control scheme for the IPC control method. Individual blade pitch angles are given by β_i with $i \in [1,2,3]$ and the out-of-blade root bending moments by M_i. The main objective of IPC is to minimize the fixed-frame tilt, M_{tilt}, and yaw, M_{yaw}, moments, which can be obtained from the blade individual moments using the MBC transform.

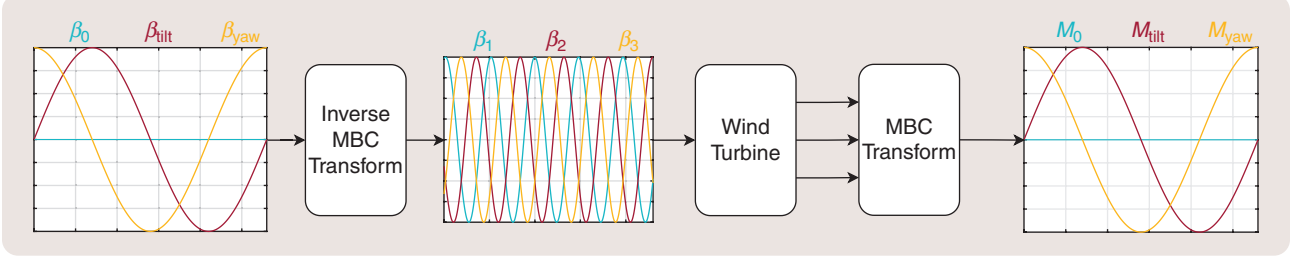

FIGURE 5 A general open-loop control scheme for the Helix wake mixing method. Contrary to IPC, the individual blade pitch angles are derived using the inverse MBC transform from the fixed-frame input signals. When applied to the turbine, the resulting fixed-frame moments are similar to the input fixed-frame blade pitch angles.

[37] are used, which are two sinusoidal inputs on both the tilt and yaw axes

$$\beta_{\text{tilt}} = A_t \sin\left(2\pi S_t \frac{V_\infty}{D} t\right) \tag{3a}$$

$$\beta_{\text{yaw}} = A_y \sin\left(2\pi S_t \frac{V_\infty}{D} t \pm \frac{\pi}{2}\right) \tag{3b}$$

in which A_t and A_y are the blade pitch angle amplitudes (in degrees), V_∞ is the free-stream wind speed (in m/s), D is the rotor diameter (in m), and S_t is a dimensionless frequency characterized by the Strouhal number. The Strouhal number is defined as

$$S_t = \frac{f_e D}{V_\infty} \tag{4}$$

in which f_e is the actuation frequency (in Hz). The phase difference $\pm\pi/2$ in (3b) determines if the Helix is applied in a clockwise or counterclockwise manner [37]. For example, the signals shown in Figure 5 are for a counterclockwise Helix [which equals to a phase lead of $\pi/2$ in (3b)]. The work in [37] shows that both clockwise and counterclockwise versions of the Helix are able to increase downstream wind speeds, but the counterclockwise version proved to be more effective. The reasons for this are a current topic of research. As such, the counterclockwise Helix will be used throughout this work.

Varying the tilt and yaw moment causes the origin of the thrust vector of the turbine to change its location with respect to the center of the turbine. This is schematically depicted in Figure 6, which shows the front view of a wind turbine. Each blade is color coded to match the individual pitch angle signals shown in Figure 5.

At any given time, each of the blades will have a different pitch angle except at certain time instants when at most two blades have the same pitch angle. The differing blade pitch angles result in different aerodynamic forces acting on each blade. As a result, the overall turbine thrust vector is no longer centered in the rotor plane but rather at an offset to the center. In Figure 6, this offset is represented by the green arrows, which also *schematically* represent the path of the resulting thrust vector during one period of the Helix. This period is an order of 10 times longer than the rotational period of the turbine, that is, when the Helix has completed one period, the turbine has rotated approximately 10 times.

Wake Mixing Background

The underlying concept of both active and passive wake mixing strategies is to augment the flow field in the wake of the wind turbine to increase the rate of entrainment of high-energy external flow into the wake induction zone. This increases turbulent diffusion and causes the wake to recover more rapidly. The near wake of a wind turbine can be characterized by coherent structures formed through the generation of lift and drag at the blade sections. The application of excitation to these structures leads to their breakdown and decay, a highly nonlinear fluid dynamic process. This excitation may occur through one of two actions: through the augmentation of the circulation of coherent structures or through the displacement of these structures. Circulation augmentation may occur through either passive means, such as the addition of blade devices that modify the wake sheet [S1], or through active means, such as through the blade pitch [37]. Circulation displacement may also occur through either passive means, such as the extension of a blade tip [S2], or through active means, such as through the modification of rotor rotational speed [S3]. A number of studies have demonstrated that wake excitation is practically achievable; however, considering the integral effect of the excitation on component fatigue, the determination of the most practical and financially feasible means of excitation is an ongoing topic of investigation.

ANALYTICAL AND NUMERICAL RESULTS

The first analytical investigation into the stability of a helical vortex system was carried out in the seminal work by Widnall [S4]. Here, it was found that three fundamental modes of instability exist: the short-wavelength, the medium-wavelength (mutual-inductance), and the long-wavelength instability. These results were extended to the multiple helix case by Gupta and Loewy [S5]. This work and further numerical analyses demonstrated that the mutual-inductance instability appears to demonstrate the highest unstable growth rate due to an initial perturbation [S5], [S6], [S7]. The influence of applying a volume force at a range of frequencies was investigated in the work of Sarmast et al. [S8]. Here, similar results were found, indicating the strong instability of the mutual-inductance mode, and an empirical formula for the transition position of the wake was derived. The impact of the motion of a floating wind turbine on the wake stability was numerically investigated in [S9], where it was shown that the motion of the platform at certain frequencies can contribute to the instability modes described previously. A numerical analysis of the helical wake excitation described in this work was carried out by [58], where it was found that both wake deflection and increased entrainment contribute to the accelerated wake breakdown and that approximately 10% more energy can be extracted from downstream turbines through the application of the helix excitation method; see Figure S1.

EXPERIMENTAL INVESTIGATIONS

The mutual-inductance instability was first observed in the smoke visualization carried out by Alfredsson and Dahlberg [S10]. The nature of the pairing instabilities and the transfer of kinetic energy over the shear layer were investigated through experiments on a small-scale rotor in an open-jet test section in Lignarolo et al. [S11], where it was identified that the vortex leapfrogging mechanism is the triggering event that accelerates

In reality, the offset is significantly smaller, typically in the order of a few meters. A major difference to the Pulse wake mixing technique is that with the Helix, the magnitude of the thrust force remains unchanged, and only the origin of the thrust force changes over time considering ideal conditions.

The effect of this moving thrust on the wake velocity profile can be seen in the wake of the rightmost turbine in Figure 2. The darker shaded area behind the turbine indicates an area of lower wind speed than the free stream, which is transparent. As the thrust vector is moving over the rotor plane, the incoming wind is most slowed down at its location. Directly opposite to the thrust vector, the local induction, that is, force opposing the incoming flow, is the lowest, resulting in the highest local wind speed. This creates a rotating area of lower and higher wind speeds that, as it moves downstream from the turbine, create a characteristic helical shape of wind speed in the wake. The Helix method obtains its name from this shape.

The area of low wind speed in Figure 2 starts to dissipate after traveling roughly four rotor diameters of distance downstream as the wake mixes with the outside flow, increasing the downstream wind speed. The effectiveness of the Helix is dependent, among other factors, on the amplitude of the blade pitch angles and its application frequency. Current research indicates that the most gain in wind speed for the Helix is achieved between $S_t = 0.30$ and $S_t = 0.40$ for a two-turbine wind farm with turbines spaced at $5D$ [54], [55]. The exact aerodynamic principle behind this is still a topic of research; see, for example, [56], [57], [58], and [59]. It should be noted that the relative gain is distance dependent. As the wake travels farther downstream, more natural mixing occurs, and the overall contribution of the Helix is lower. Closer to the turbine, the natural mixing process has not started yet, and the wind speed in the wake is still low.

Typically, research into wake mixing methods focuses on increasing the energy of a turbine located at a distance of five rotor diameters. On average, the spacing in current offshore wind farms is 10 rotor diameters [60], [61]. Furthermore, if significant gains in power production can be achieved for distances closer to the upstream turbines, it is also feasible to pack more turbines within the same wind farm, further increasing its power production.

For bottom-fixed turbines, the Helix has shown significant potential to mitigate the turbine-to-turbine wake recovery. Both long-wavelength and short-wavelength instabilities were experimentally generated in the work of Leweke et al. [S12]. The influence of displacement perturbations of the vortex structure was investigated by Quaranta et al. [S3], where it was demonstrated that the local pairing of vortices is the driving factor behind the instability of a helical wake system and that the leapfrogging results from global vortex pairing modes.

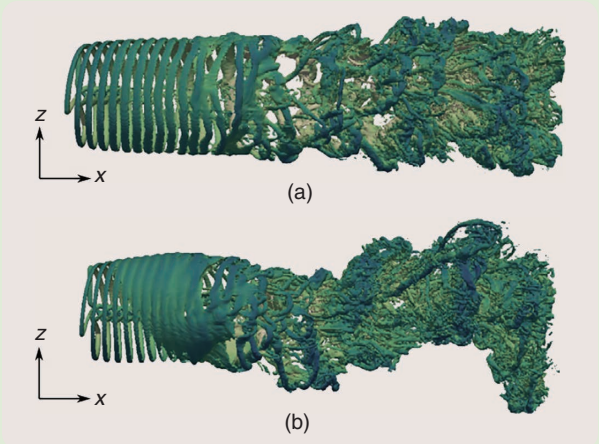

FIGURE S1 (a) The vorticity isocontour of a wind turbine wake in standard control operation and (b) with helix wake excitation. (Source: Taken from [58].)

REFERENCES

[S1] D. Schröder, T. Leweke, R. Hörnschemeyer, and E. Stumpf, "Generation of a wingtip vortex pair using a pressure-side fin," *Aerosp. Sci. Technol.*, vol. 130, Art. no. 107860, Nov. 2022, doi: 10.1016/j.ast.2022.107860.

[S2] N. Ramos-García, A. Abraham, T. Leweke, and J. N. Sørensen, "Multi-fidelity vortex simulations of rotor flows: Validation against detailed wake measurements," *Comput. Fluids*, vol. 255, Apr. 2023, Art. no. 105790, doi: 10.1016/j.compfluid.2023.105790.

[S3] H. U. Quaranta, M. Brynjell-Rahkola, T. Leweke, and D. S. Henningson, "Local and global pairing instabilities of two interlaced helical vortices," *J. Fluid Mech.*, vol. 863, pp. 927–955, Jan. 2019, doi: 10.1017/jfm.2018.904.

[S4] S. Widnall, "The stability of a helical vortex filament," *J. Fluid Mech.*, vol. 54, no. 4, pp. 641–663, 1972, doi: 10.1017/S0022112072000928.

[S5] B. P. Gupta and R. G. Loewy, "Theoretical analysis of the aerodynamic stability of multiple, interdigitated helical vortices," *Amer. Inst. Aeronaut. Astronaut.*, vol. 12, no. 10, pp. 1381–1387, 1974, doi: 10.2514/3.49493.

[S6] M. J. Bhagwat and J. Leishman, "Stability, consistency and convergence of numerical algorithms for time-marching free-vortex wake analysis," *J. Amer. Helicopter Soc.*, vol. 46, no. 1, pp. 59–70, 2001, doi: 10.4050/JAHS.46.59.

[S7] G. Leishman, M. J. Bhagwat, and S. Ananthan, "The vortex ring state as a spatially and temporally developing wake instability," *J. Amer. Helicopter Soc.*, vol. 49, no. 2, pp. 160–175, 2004, doi: 10.4050/JAHS.49.160.

[S8] S. Sarmast et al., "Mutual inductance instability of the tip vortices behind a wind turbine," *J. Fluid Mech.*, vol. 755, pp. 705–731, Aug. 2014, doi: 10.1017/jfm.2014.326.

[S9] V. G. Kleine, L. Franceschini, B. S. Carmo, A. Hanifi, and D. S. Henningson, "The stability of wakes of floating wind turbines," *Phys. Fluids*, vol. 34, no. 7, Jul. 2022, Art. no. 074106, doi: 10.1063/5.0092267.

[S10] P. H. Alfredsson and J. A. Dahlberg, "A preliminary wind tunnel study of windmill wake dispersion in various flow conditions," National Aeronautics and Space Administration, Washington, DC, USA, Tech. Rep. AU-1499, 1979.

[S11] L. Lignarolo, D. Ragni, F. Scarano, C. Simão Ferreira, and G. van Bussel, "Tip-vortex instability and turbulent mixing in wind-turbine wakes," *J. Fluid Mech.*, vol. 781, pp. 467–493, Sep. 2015, doi: 10.1017/jfm.2015.470.

[S12] T. Leweke, H. Quaranta, H. Bolnot, F. Blanco-Rodriquez, and L. L. Dizes, "Long- and short-wave instabilities in helical vortices," *J. Phys., Conf. Ser.*, vol. 524, no. 524, 2014, Art. no. 012154, doi: 10.1088/1742-6596/524/1/012154.

interaction. The time-varying moments that are applied to the turbine using the Helix method will interact with a floating structure. When a tilt moment is applied, the turbine will likely change its floater pitch angle, changing the inflow angle. When a yaw moment is applied, the floating turbine will yaw, resulting in the yaw misalignment of the turbine with respect to the flow. These movements will affect the flow behind the turbine. Furthermore, the misalignment of the turbine with respect to the incoming flow creates a tangential force component at the location of the rotor thrust vector. Either or both of these effects can potentially influence the wind speed downstream, be it by affecting the wake mixing technique directly or by interacting with the aerodynamic mixing process.

COUPLING BETWEEN THE HELIX METHOD AND THE INTERNATIONAL ENERGY AGENCY 15-MW FLOATING TURBINE MOTIONS

This section provides an in-depth analysis of the movements of the International Energy Agency (IEA) 15-MW turbine [62] mounted on the VolturnUS-S floater [63] when using the Helix method. To gain a better understanding of the coupling, the frequency-response functions are analyzed. These responses are obtained from input–output data acquired from identification experiments [64]. The identified response functions provide insight into how the platform dynamics of the floater and the dynamics of the Helix couple. The frequency-response data give insight into the dynamics of a single turbine and how it interacts with the Helix method but not the impact on the wake mixing process. The influence of the resulting motion on the wake is discussed in the next section.

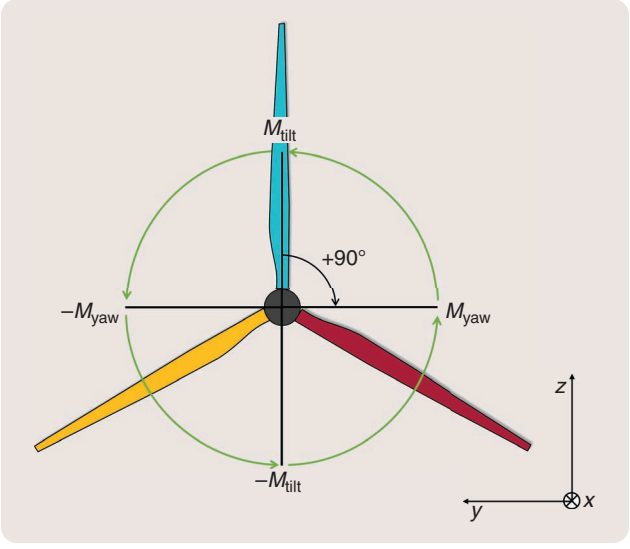

FIGURE 6 The front view of the rotor plane of a wind turbine. As each blade is pitched the thrust vector will move, off-center, clock, or counterclockwise over the rotor plane. This dynamic induction zone promotes the onset of wake mixing.

Simulation Tools and Research Methodology

All investigations presented in this research are conducted using QBlade [49]. QBlade is capable of simulating coupled aerodynamics, structural dynamics, and hydrodynamics. To model the turbine and wake aerodynamics, a free-wake vortex method is used. The vortex method was originally developed for modeling the wake of helicopter rotors [65], [66]. Its benefits over comparable computational fluid dynamic methods primarily come from being computationally more efficient without major loss of accuracy [67].

The free vortex method as used in QBlade can be viewed as a low-cost alternative method of simulating the wind turbine wake. The majority of the research investigating the wakes of individual wind turbines or wind farms uses some form of large-eddy simulations (LESs) to investigate near- and far-wake behavior while being reasonably efficient. However, for LESs, the whole domain needs to be discretized with finite-volume elements. In general, reducing the size of these volume elements increases the accuracy of the resolved wake at the cost of growth in computational costs.

The free vortex method models the wake and flow field using a Lagrangian approach. These methods have previously successfully been used to model wind turbine wakes [68], [69], [70], [71], [72]. In [72], the predicted wake breakdown location is analyzed using the same free vortex wake (FVW) code as used in this work. It is compared to an identical simulation carried out in LES and other literature data. It was observed that the transition position aligns well with the predictions of LES modeling. Beyond the point of transition, however, the lifting line FVW model does not accurately capture the effect of turbulent diffusion. Furthermore, the same work also describes how the actuation of flaps located near the tip of the blade can accelerate the tip-vortex pairing, a process that instigates wake breakdown. Finally, it also proposes a solution to improve upon the accuracy of the current implementation of the FVW method.

An important distinction between [72] and this work is that the frequency at which the control is implemented is an order of magnitude lower for the Helix method compared to the flap control used in [72]. As this work focuses on the behavior of the wake near the upstream turbine and only up to five D downstream, the free-wake vortex method can be used. To understand the wake behavior, a quantitatively accurate method such as LES is required to validate these approaches and explore more accurately the impact of turbulent statistics in the posttransition region.

The IEA 15-MW [62] on the VolturnUS-S [63] floater, as modeled in QBlade, can be seen in Figure 7, including part of the wake represented by the free vortex elements. For every simulation conducted in this work, the inflow wind speed is uniformly distributed and set at 9 m/s. This represents an ideal case scenario for the wake mixing strategy. At this wind speed, the turbines are operating in below-rated conditions and extract all available energy from the flow. In above-rated conditions, there is typically

enough energy in the flow behind the turbine that any waked downstream turbines can also operate near or at the rated power [27], [73]. A further reason for choosing a fixed wind speed is that the excitation frequency, defined by the Strouhal number, (4), is wind speed dependent. Considering multiple wind speeds would complicate the analysis and increase the number of simulations.

Finally, the flow is considered to be laminar. When turbulent inflow is used, natural mixing occurs in the wake. This reduces the relative effectiveness of the wake mixing technique. However, wake mixing can still be beneficial even when turbulence is considered. The works in [58] and [59] use synthetic turbulence in their simulations, that is, turbulence is superposed onto a mean inflow. For both works, the turbulence intensity (TI) is around 5%. Similarly, work on the Helix in [37] and [57] includes turbulence developed in an atmospheric boundary layer. In [37], the TI is set to 5% over the whole domain, whereas [57] uses a TI that varies between 3% at the top of the turbine and 5.8% at the bottom. What these four investigations have in common is that the turbulence level is relatively low. It is expected that this control strategy will be applied in conditions with a TI level in this range as it is most effective for those conditions. Omitting turbulence from the simulation enhances the effect of the Helix method on the wake, allowing for an easier comparison of the wake behavior between that of a bottom-fixed turbine and a floating turbine.

For the simulations of the floating turbine, a wave field is included in the simulation. The presence of a wind field above a still body of water will generate waves [74], so-called wind-swept waves. The exact nature of the waves is site dependent and is determined through site-specific assessments. When site-specific information is not available during the design phase of the turbine, the IEC 61400-3-1:2019 Standard can be used [75]. The table with wind speeds and associated wave parameters can be found in [63, Tab. 12]. The size and frequency content of these waves is parameterized using a JONSWAP wave spectrum [76]. For the interested reader, a detailed description of QBlade can be found in "Aero-Servo-Hydroelastic Models in QBlade." The specific settings used in this work can be found in "Detailed Numerical Setup Description."

Frequency-Domain Analysis

To capture the dynamics of the IEA 15-MW floating turbine, the system is excited using a chirp signal. This signal is chosen such that it excites the system over $1{\cdot}10^{-3}$ to the 1-Hz frequency range. The input is logarithmically distributed over the full duration of the experiment such that more of the data collected is generated at lower frequencies. The full experiment produces 28,800 s (8 h) of data. In previous work, it was identified that for semisubmersible platforms, like the VolturnUS-S platform, the yaw motion is dominant [47]. For that reason, the chirp is applied to the fixed-frame β_{yaw} input.

Figure 8 shows the frequency response for all six degrees of freedom of the floating turbine as a function of the blade pitch angle. The data are presented as the ratio between the

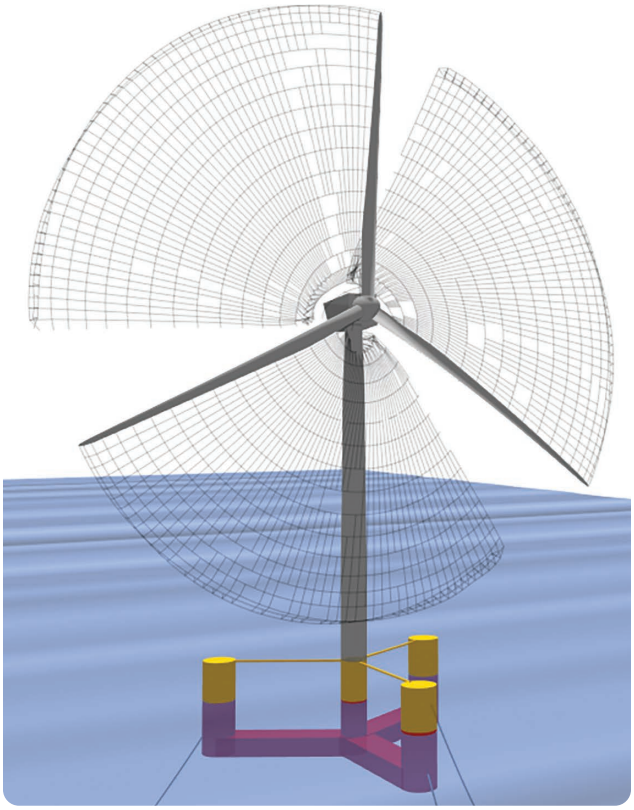

FIGURE 7 A close-up of the IEA 15-MW turbine on the VolturnUS-S floater in QBlade. The image is taken at the start of the simulation at which only the near wake is visible, represented by the black lines, which are vortex elements released in the wake.

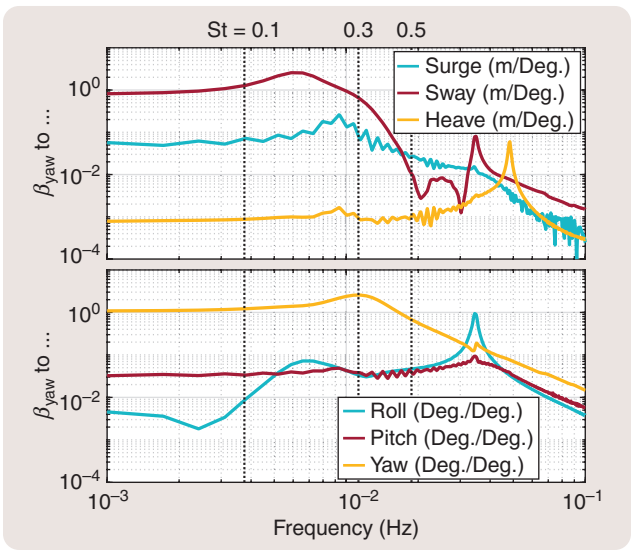

FIGURE 8 The frequency responses for the IEA 15-MW turbine on the VolturnUS-S semisubmersible platform for all six degrees of freedom. The vertical dotted lines represent the frequencies for three different Strouhal numbers. At different actuation frequencies, the platform will undergo differing types of motion. Deg.: degree.

Aero-Servo-Hydroelastic Models in QBlade

QBlade is a comprehensive software that enables the design and simulation of dynamics for both bottom-fixed and floating wind turbine systems [49]. When simulating floating wind energy systems, it is crucial to account for the intricate interplay between various aspects, such as aerodynamics, hydrodynamics, and control mechanisms, and the effects of elastic, inertial, and gravitational loads. These interactions often result in highly nonlinear behaviors, which can be counterintuitive and differ significantly from the responses observed in land-based bottom-fixed wind turbines. To gain a deep understanding of these inherent couplings, it is imperative to explicitly resolve the nonlinear dynamics in the time domain as simplified linearized models often fall short. QBlade is designed as a medium-fidelity simulation code that can predict coupled system dynamics in real time or faster. This requirement has profound implications when it comes to choosing suitable numerical models capable of accurately resolving the relevant system dynamics; see Figure S2.

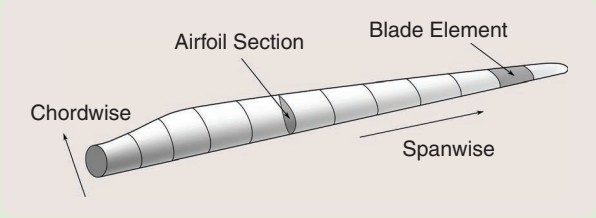

FIGURE S2 2D airfoil sections and the discretization of a rotor blade into 2D elements.

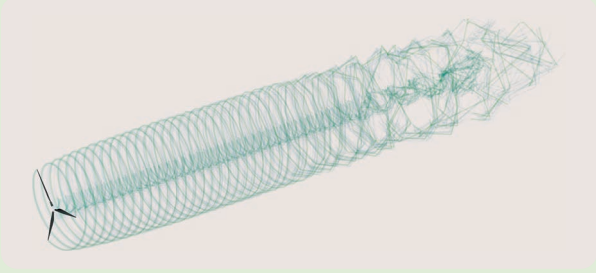

FIGURE S3 The helical rotor wake structure discretized with Lagrangian vortex filaments. The onset of wake breakdown is visible far downstream.

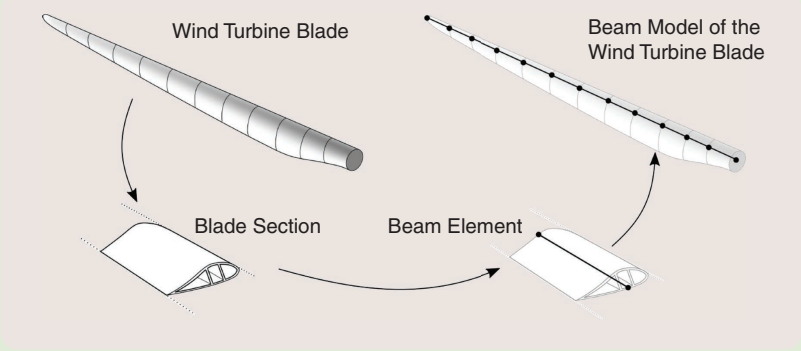

FIGURE S4 The reduction of a complete composite blade structure into blade sections and beam elements.

AERODYNAMICS

As in most numerical approaches, the modeling of aerodynamics can be broken down into two main aspects: the modeling of aerodynamic forces on the turbine blades and the modeling of rotor wake aerodynamics. Due to computational constraints, fully resolved 3D computational fluid dynamics simulations of the blades are not feasible for long-duration time-domain analyses. Therefore, the commonly adopted blade element approach [S13] involves representing blade loads using precomputed lift, drag, and moment coefficient polars. These polars capture the aerodynamic characteristics of a 2D airfoil section across various angles of attack. The polar data can be obtained through wind tunnel experiments or numerical simulations. By spatially integrating the 2D polar data along the blade span, the rotor blade, which usually consists of multiple airfoil sections, can be effectively represented.

When aerodynamic forces act on the rotor, kinetic energy is extracted from the flow, leading to a reduction in flow velocity as it traverses the rotor disk. This localized region of reduced flow velocity is referred to as the *rotor wake*. The mechanism behind this energy extraction involves the formation of a helical vortex system trailing behind the rotor. The rotational motion of the vortex induces circular movement in neighboring fluid particles. The combined effect of this vortex system is a decrease in the flow velocity downstream of the wind turbine rotor. QBlade incorporates the explicit modeling of this vortex system using Lagrangian vortex filaments, whose convective velocity is updated and integrated at every time step [S14]. An example of such a wake can be seen in Figure S3 These filaments, which are shed from the rotor blades based on their aerodynamic loading, exert an influence on all other vortex filaments and on the rotor itself. By considering the collective impact of all wake vortex filaments at any given point in space, the induced velocities in the wake region can be accurately evaluated. It is worth noting that the rotor wake also significantly affects the velocities at the position of the rotor blades themselves as well as the evolution of the wake itself: a phenomenon known as *wake roll-up*.

STRUCTURAL DYNAMICS AND CONTROL

QBlade utilizes the versatile open source library Project-Chrono [S15] as a middleware for modeling and solving the structural dynamics of wind turbines. The approach for modeling structural dynamics involves representing the elastic and slender components of wind turbine parts (such as the tower and blades)

using beam elements. These beam elements are interconnected in a multibody formulation to represent the entire structure of the wind turbine. Each beam element is assigned properties such as mass, stiffness, and damping, which capture its complex composite structure and may vary along the length of each element.

By using beam elements, the complete structure of a wind turbine can be represented with a manageable number of degrees of freedom, typically in the order of thousands. This is in contrast to a full finite element analysis approach, which would require millions of degrees of freedom. Despite the reduced complexity, the beam element representation still provides accurate results when resolving the coupled response of the structural system. Additionally, the flexible beam element formulation can be combined with lumped masses and rigid bodies that may represent nondeformable parts of the system, such as the floating substructure of the turbine, which is typically not susceptible to significant elastic deformations. A combination of such a setup is shown in Figure S5.

Within the multibody system of the wind turbine, various components are connected through actuators. For example, the blade elements are linked to the blade hub using rotational actuators, representing the pitch drive mechanism. Another example is the generator, which applies an opposing torque onto the main shaft connected to the rotor hub. These actuators receive signals from controller libraries that contain the complete control logic of a wind turbine, including algorithms for supervisory control tasks such as emergency shutdown events that are triggered by specific thresholds. The controller libraries operate alongside the structural simulation, receiving inputs and sending control signals to the actuators of the structural model; a schematic representation of this interface is seen in Figure S6. The signals could be related to blade pitch (as utilized in this study), rotor yaw, emergency brake activation, or other actuators distributed over the wind turbine system.

HYDRODYNAMICS

QBlade incorporates two medium-fidelity methods to simulate hydrodynamic forces on offshore structures: the Morison equation combined with strip theory and a model based on linear potential flow hydrodynamics. The empirical Morison equation [S17] estimates the forces and moments on a submerged body in a wave field. The Morison equation contains three essential terms for estimating hydrodynamic forces: the inertia, hydrodynamic mass, and drag term. The hydrodynamic inertia captures the effects of fluid acceleration or deceleration around the structure.

The added mass accounts for the additional mass of fluid that contributes to the dynamic response of the body. The hydrodynamic drag term considers the quadratic drag experienced by the structure as it moves through the fluid. When combined with strip theory, which divides complex structures into slender strips, the Morison equation can estimate distributed hydrodynamic forces across the entire structure; see Figure S7. However, the Morison equation falls short in predicting the hydrodynamic interactions between the individual components

FIGURE S5 A representation of a floating wind turbine with beam elements connected in a multibody formulation.

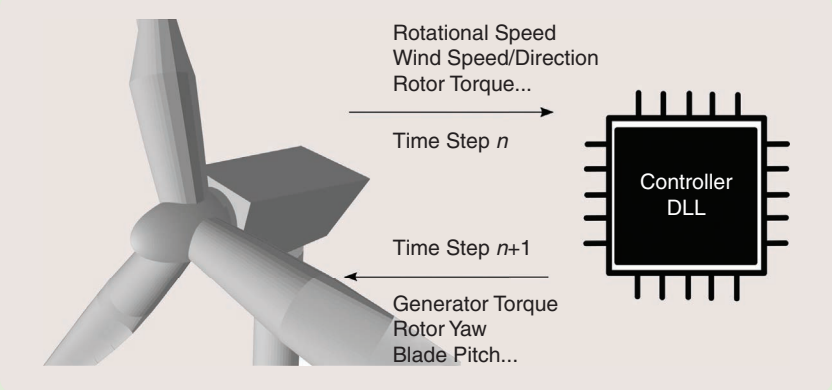

FIGURE S6 The communication between the controller and the turbine. DLL: dynamic linked library.

(*Continued*)

Aero-Servo-Hydroelastic Models in QBlade (*Continued*)

of the same structure as each strip is solved independently. Additionally, it has limited accuracy for nonslender structures.

In contrast, the linear potential flow method [S18] employed in QBlade predicts the combined hydrodynamic excitation and radiation forces on the complete structure, assuming inviscid flow. This method relies on a preprocessed hydrodynamic response database obtained from potential flow solvers such as WAMIT [S19], NEMOH [S20], and Ansys AQWA [S21]. During a simulation, this frequency-domain hydrodynamic database is converted into the time domain. One drawback is that the potential flow method typically calculates the hydrodynamic response for a single reference point, lumping together all forces and moments. As a result, it does not provide a distribution of hydrodynamic forces required to model hydroelastic effects. However, since most floating structures are relatively rigid compared to soft and slender rotor blades, they are often modeled as rigid bodies with accurate mass and inertial properties—thereby capturing their dominant contributions to the overall system response. Figure S8 shows the IEA 15-MW turbine modeled as a rigid body in an irregular wave field.

It is important to note that the potential flow theory assumes inviscid flow and therefore cannot predict quadratic hydrodynamic drag. To incorporate drag into the simulation, the potential flow method may be combined with the Morison-based strip theory. This hybrid approach provides a more comprehensive representation of the total hydrodynamic forces.

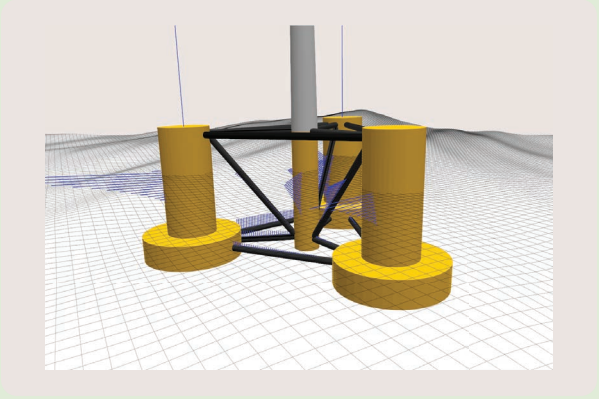

FIGURE S7 Distributed Morison drag forces, in blue, acting on the DeepCwind [S16] floater operating in a multidirectional and irregular wave field.

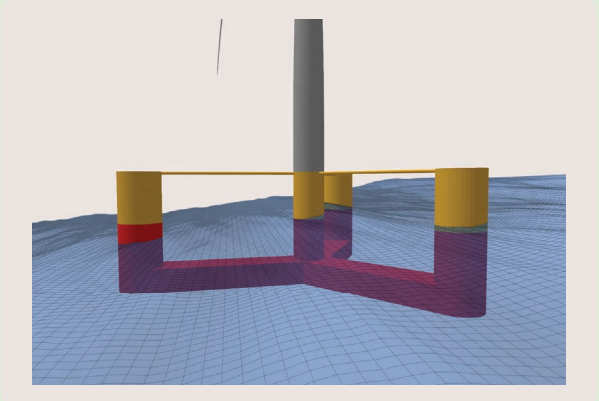

FIGURE S8 A rigid body, potential flow model of the VolturnUS-S floater operating in a multidirectional irregular wave field.

REFERENCES

[S13] H. Glauert, "The elements of aerofoil and airscrew theory," *Roy. Soc.*, vol. B144, no. 877, pp. 73–93, 1935.

[S14] D. Marten, M. Lennie, G. Pechlivanoglou, and C. O. Paschereit, "Implementation, optimization, and validation of a nonlinear lifting line-free vortex wake module within the wind turbine simulation code QBlade," *Trans. ASME, J. Eng. Gas Turbines Power*, vol. 138, no. 7, 2016, Art. no. 072601, doi: 10.1115/1.4031872.

[S15] A. Tasora et al., "Chrono: An open source multi-physics dynamics engine," in *Proc. Int. Conf. High Perform. Comput. Sci. Eng.*, 2016, pp. 19–49.

[S16] A. Robertson et al., "Definition of the Semisubmersible Floating System for Phase II of OC4," National Renewable Energy Lab. (NREL), Golden, CO, USA, Tech. Rep. TP-5000-60601, 2014.

[S17] J. R. Morison, M. P. O'Brien, J. W. Johnson, and S. A. Schaaf, "The force exerted by surface waves on piles," *J. Petroleum Technol.*, vol. 2, no. 05, pp. 149–154, 1950, doi: 10.2118/950149-G.

[S18] J. N. Newman, *Marine Hydrodynamics*, 2nd ed. Cambridge, MA, USA: MIT Press, 1977.

[S19] C. M. Lee and J. N. Newman. "The WAMIT user manual." Wamit. Accessed: Aug. 08, 2024. [Online]. Available: http://www.wamit.com

[S20] R. Kurnia and G. Ducrozet, "NEMOH: Open-source boundary element solver for computation of first- and second-order hydrodynamic loads in the frequency domain," *J. Comput. Phys. Commun.*, vol. 292, Nov. 2023, Art. no. 108885.

[S21] "ANSYS AQWA user's manual." ANSYS. Accessed: Aug. 08, 2024. [Online]. Available: https://www.ansys.com/training-center/course-catalog/structures/introduction-to-hydrodynamic-analysis-with-ansys-aqwa

input and output spectra. Beyond 0.1 Hz, the system becomes insensitive to any input, which is the reason the data are displayed up to 0.1 Hz even though the system is excited to 1 Hz. Included in Figure 8 are vertical lines at three frequencies typically considered for wake mixing. The corresponding Strouhal number for the IEA 15-MW turbine is annotated above the dashed lines. Between $S_t = 0.10$ and $S_t = 0.50$, the wake mixing process is most effective. Higher Strouhal numbers result in less effective wake mixing as the blade pitching is no longer triggering the wake instabilities.

In terms of absolute gain, two of the six degrees of freedom are excited almost equally. These are the sway and yaw motions, both with a peak gain of 2.5 albeit at different frequencies. However, given the scale of the turbine, the absolute displacement of the sway motion can be considered negligible. For example, if the Helix were applied with a 4° blade pitch amplitude on both fixed-frame coordinates, the turbine

would displace at most 10 m, which is considered small compared to the rotor diameter. On the contrary, the same input results in $\pm 10°$ of yaw misalignment, which can be considered a sizeable yaw misalignment angle. Aside from these two motions, the remaining four degrees of freedom are excited at an order of magnitude smaller or are excited at frequencies outside the range of interest for wake mixing.

The presence of waves will also cause the platform to undergo a degree of motion. However, wave excitation often occurs in a frequency range an order of magnitude higher than that of the Helix. When designing a floating vessel, response amplitude operators (RAOs) are constructed to represent the response of the vessel to wave inputs at different frequencies [77]. For the VolturnUS-S reference platform, the RAOs can be found in [63]. The platform motions for a wavefield with a similar wave height as used in this work are small such that their impact on the wake is negligible. Especially in yaw, the Helix-induced yaw motion will be significantly larger than that of the wave forces.

From the frequency-response data, it is possible to evaluate if the yawing motion affects the Helix method. This can be measured by evaluating the transfers from the fixed-frame blade pitch angles to the fixed-frame tilt and yaw moments. These transfer functions provide insight into the full coupling between the aero- and platform dynamics. The relations between blade pitch input and fixed-frame tilt and yaw moments are shown in Figure 9, where the data for M_{tilt} and M_{yaw} are normalized with respect to the maximum value of M_{yaw}. In the same figure, the response of the yaw motion to β_{yaw} is also included.

Even though the experiment uses only the β_{yaw} input, there is still a response on the M_{tilt} axis. Hence, a coupling exists between the fixed-frame yaw and tilt axis with this implementation of the MBC transform. This can be solved by including an azimuth offset in the transformation [52]. When the yaw motion is small (gain ≈1 or lower), the gain for the yaw moment remains constant. However, at the eigenfrequency of the yaw motion, there is a small antiresonance in the yaw moment. Coincidentally, the frequency range where the yaw motion is most prominent is also the frequency range where the Helix is most effective.

The investigation presented in this section indicates that there exists a two-way coupling between the dynamics of the Helix and the platform dynamics of the floating turbine. The yaw movement of the floating turbine reduces the yaw moment of the Helix. The impact that this has on the wake mixing behind the turbine will be investigated in the following section.

TIME-DOMAIN ANALYSIS OF WAKE RECOVERY

This section will analyze the dynamics of the wake mixing process and whether the yaw movement has any impact on it. This is done by comparing the wind speed downstream of the turbine for different Strouhal numbers. Wake recovery can be evaluated by comparing the wind speed at different distances downstream to a baseline case. Furthermore, all simulations will be run for two different amplitudes for the blade pitch angles to assess the impact of different blade pitch angles.

For comparison, the same simulations will be executed for a bottom-fixed version of the IEA 15-MW turbine. By comparing the simulations for a floating turbine to those of a bottom-fixed turbine, the impact of the motion can be better analyzed. First, the simulation cases will be introduced as well as the metrics that are being analyzed. Second, the results of the simulations are presented.

Time-Domain Simulation Scenarios

All simulations carried out in this work were done using the software-in-the-loop interface of QBlade [78]. The settings, as described in "Detailed Numerical Setup Description," were used for all simulations. The total simulation time for each simulation was 1,600 s, of which the first 400 s were omitted to remove transients from the simulation initialization. The remaining 1,200 s were used for the data analysis.

For the baseline case, both the bottom-fixed and floating turbines have their blade pitch angle set to 0°. Maximum power extraction is achieved by employing a $k\omega^2$ controller that controls the generator torque such that the turbine operates at the optimal tip-speed ratio [79]. For each simulation, the wind speed is retrieved at the following distances:

$$D = [-1.0\ 0.0\ 1.0\ 2.0\ 2.5\ldots \\ \ldots 3.0\ 3.5\ 4.0\ 4.5\ 5.0\ 6.0]. \tag{5}$$

As the floating turbine has a steady-state surge offset, an offset of ≈16 m is applied to (5). The average wind speed is retrieved at the points shown in Figure 10. This number of points was

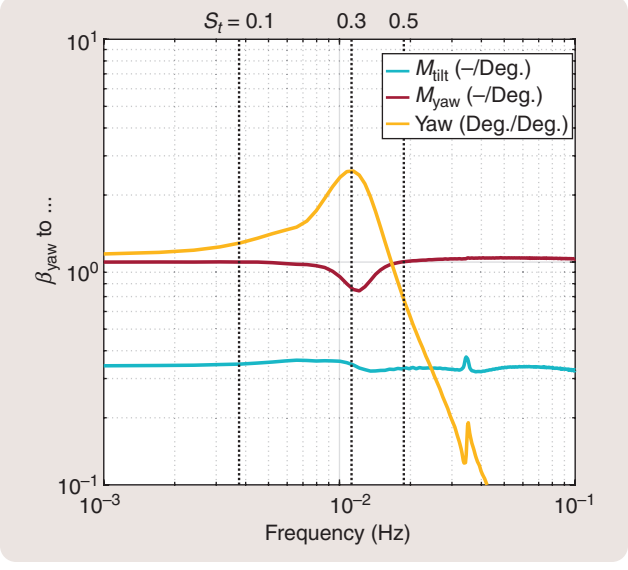

FIGURE 9 The frequency responses showing the gain in yaw motion and the gain in M_{tilt} and M_{yaw}. The M_{tilt} and M_{yaw} responses are normalized with respect to the maximum value of M_{yaw}. The vertical dotted lines represent the frequencies for 3 different Strouhal numbers.

Detailed Numerical Setup Description

This section will motivate the settings and their respective values used in QBlade. The spatial resolution of a wake modeled by the free-wake vortex approach is dictated by the number of vortex elements in the wake. The settings used in this work are based on those used in [45] or differ slightly to speed up the initial transients of the wake to reduce the computational time. For that work, the parameters were selected based on a convergence study, which is also relevant to this work.

The settings that influence this tradeoff can be subdivided into three subcategories, each affecting a different aspect of the simulation. The first category falls under wake modeling and primarily determines the length of the wake. The second category is vortex modeling. Its parameters influence the behavior and interaction between the individual vortex elements in the wake. The third category covers turbine modeling. This category has less of a direct influence on the wake behavior but is still important for computational efficiency and, to a lesser degree, accuracy.

The wake modeling settings are summarized in Table S1. These settings function as a hard limit on the number of wake elements. If more elements are created than these maxima allow, the older elements in the wake are removed from it. This hard limit can be defined either by a maximum number of elements or by allowing the elements to stay in the wake for a distance defined in rotor diameters, whichever comes first for a particular simulation. Wake relaxation blends out the starting vortex by controlling the wake length given a number of rotor revolutions. For example, the factor of 0.8 implies that after one revolution, the wake generated in the first 0.2 revolutions has been removed. This reduces the large transients in the wake that are associated with the starting vortex that is generated at the initialization of each simulation run.

The wake reduction factor removes each vortex element whose vorticity strength is smaller than the product of the reduction factor times the maximum vorticity present in the wake. Elements below this threshold hardly impact wake dynamics and can be removed to speed up the simulation. The final two settings, the near wake and zone 1/2/3 length, are zones where the wake gradually becomes coarser. As the wake transitions between zones, vortex elements are merged by a wake zone factor, two for all zones in this work, to again speed up the simulation.

TABLE S1 Wake discretization settings.

Wake Modeling	Setting
Wake relaxation	0.8
Max. wake elements	200,000
Max. wake distance	100 rotor diameters
Wake reduction factor	0.001
Near wake length	0.5 revolutions
Wake zone 1/2/3 length	6/12/6 revolutions
Wake zone 1/2/3 factor	2/2/2

Max.: maximum.

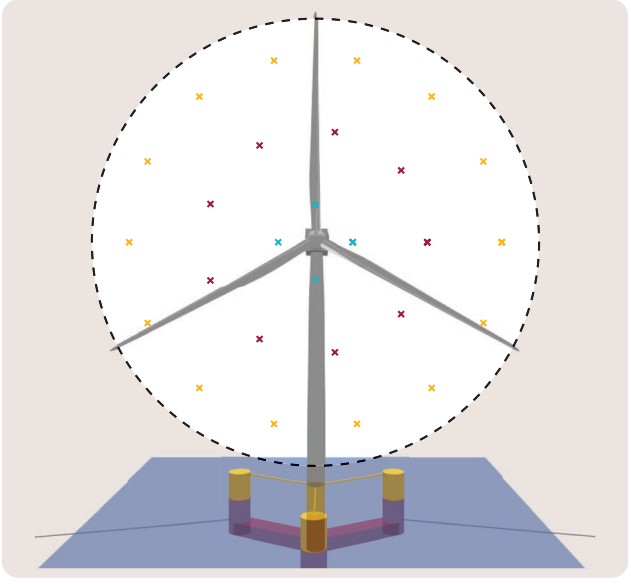

FIGURE 10 The front view of the IEA 15-MW turbine mounted on the VolturnUS-S platform with the points at which the wind speed is measured. The rotor-swept area is indicated by the dashed circle.

found to be a good tradeoff between computational expense and accuracy. The average wind speed as measured at these locations provides insight into the potential power production for a second downstream turbine.

The Helix is applied with a blade pitching amplitude of 2° and 4°. At these amplitudes, the wake mixing process will be triggered by the Helix method, and at the same time, it provides insight into a potential nonlinear relation between yaw motion and the Helix method. It could be that at smaller platform yaw angles, it provides a benefit that is diminished at larger yaw angles. To investigate the impact of the motion, the application frequencies used in this work cover the full range in which wake mixing is effective. The following Strouhal numbers were chosen:

$$S_t = [0.00\ 0.10\ 0.15\ 0.20\ 0.25\ 0.30\ldots \\ \ldots 0.35\ 0.40\ 0.45\ 0.50\ 0.60\ 0.70] \quad (6)$$

in which $S_t = 0.00$ represents the baseline case. Research indicates that an optimum frequency exists for wake mixing that is dependent on the distance to the next downstream

TABLE S2 Aerodynamic modeling settings.

Vortex Modelling Settings	Setting
Fixed bound core radius	0.05% Chord
Initial core radius	0.05% Chord
Vortex viscosity coefficient	900 [–]
Max. vortex stretching factor	50 [–]
Trailing vortices	Enabled
Shed vortices	Enabled

TABLE S3 Turbine modeling settings.

Turbine Settings	Setting
Dynamic stall model	ATEFlap
Time constant T_f	3.0 [–]
Time constant T_p	2.0 [–]
Time step	0.05 [s]
Azimuthal step	$\Delta\psi = 19°$ [deg]
Inflow velocity	9 m/s
Discretization panels (no.)	20 [–]
Discretization method	Sinusoidal

The settings for vortex modeling are summarized in Table S2. The magnitude of the interaction between vortex elements scales with the inverse of the distance between them. To prevent extreme values when two vortices are near each other, each vortex element is given a core radius, which is an area around the vortex elements in which this interaction is artificially scaled down. This core size changes as the wake travels downstream. Increasing the core size decreases the mutual interaction among elements in the wake and emulates the effects of diffusion. The vortex stretching factor removes vortices that have grown more than that factor past their initial size. The vortex viscosity coefficient is set to 900, which was found to work well for modeling large rotors [S22], [S23]. Finally, having both trailing and shed vortices allows for capturing both spatial and temporal vorticity gradients in the wake.

Table S3 summarizes the turbine modeling settings used in all simulations. The time step for each simulation is set to 0.05 s. This results in an azimuthal step of the turbine of $\Delta\psi = 1.9^{\circ}$ with an inflow velocity of 9 m/s. Smaller azimuth steps may lead to higher accuracy; at every azimuth step, vortices are released, but this comes at the cost of computational time [67]. Finally, the blade is discretized in 20 panels, which are sinusoidally distributed over the blade. For the unsteady blade aerodynamics, the ATEflap model is used with the given T_f and T_p constants.

REFERENCES

[S22] S. Ananthan and J. G. Leishman, "Role of filament strain in the free vortex modeling of rotor wakes," *J. Amer. Helicopter Soc.*, vol. 49, no. 2, pp. 176–191, 2004, doi: 10.4050/JAHS.49.176.

[S23] T. Berdowski, "Three-dimensional free-wake vortex simulations of an actuator disc in yaw and tilt," in *Proc. Wind Energy Symp.*, 2018, Art. no. 0513, doi: 10.2514/6.2018-0513.

turbine. For DIC, this is $S_t = 0.25$ for a two-turbine wind farm spaced at five rotor diameters [35]. By evaluating the wind speed over the distance (5) and Strouhal number (6), this ideal frequency can be found for the Helix. Furthermore, comparing the data from bottom-fixed and floating turbines can provide insight into whether the optimum changes are due to the extra dynamics of a floating turbine.

Time-Domain Simulation Results

The results will be presented in three different sections. First, the yaw motion and yaw- and tilt moment for both blade pitch amplitudes will be shown. For these datasets, three different Strouhal numbers are chosen. These Strouhal numbers represent the system behavior before, at, and after the eigenfrequency. Furthermore, the time-domain data at these three frequencies can be used to verify the results found using the frequency-response functions. Secondly, the average wind speed downstream is evaluated. By looking at the wind speed downstream and comparing it to the baseline case, the accelerated wake recovery can be quantified. Finally, the average aggregated power production of the two-turbine wind farms is compared. Higher actuation frequencies and larger amplitudes lead to a loss in the power production of the actuated turbine. Furthermore, if an optimum exists for wake recovery, that is, a Strouhal number and distance where the relative gain in wind speed is largest, this combination of Strouhal and distance does not necessarily result in the highest gain of power production.

Turbine Time-Domain Response

The yaw motion for the three different Strouhal numbers and both blade pitch amplitudes are shown in Figure 11. The time range shown is equal to one period for $S_t = 0.10$. Included in Figure 11 is the yaw motion for the baseline case. The incoming waves do not perturb the turbine such that they create any significant yaw motion. This is for two reasons. First, the wave field used is aligned with the incoming flow and does not excite the yaw degree of freedom. Second, the wave field used represents a calm sea for this wind condition, and therefore, the wave forces are relatively small.

The amplitude in yaw motion for the 2° input peaks at 6°. This is higher than the expected amplitude based on the gain

found in the frequency-response experiment. For the 4° input, the amplitude of the yaw motion matches the gain as the identification input is 4°. The greater-than-expected motion at 2° can be explained by the fact that both the stiffness and damping of a floating vessel are dependent on the amplitude and velocity of the motion [77]. At the lower blade pitch amplitude, the platform has a lower yaw velocity, and thus, the interaction between the floater movement and the water is different compared to the 4° case. This nonlinear behavior of the stiffness and damping can be one of the reasons why there is a difference in expected versus actual yaw amplitude.

The tilt and yaw moments for the bottom-fixed and floating turbines are shown in Figures 12 and 13. For the tilt moment (see Figure 12), there are only small differences in peak-to-peak amplitude when comparing the floating and bottom-fixed turbines. This can potentially be put down to the nacelle moving forward and backward due to wave-induced motion or the applied tilt moment. The larger yaw movement does have an impact on the yaw moment that is generated by the Helix.

Figure 13 shows the comparison of the yaw moment for the bottom-fixed and floating turbine. When actuated at $S_t = 0.30$, there is a significant reduction in yaw moment, which confirms the frequency analysis. The reduction in yaw moment can be explained by the fact that as the turbine is undergoing yaw motion, part of the turbine is moving away from the incoming flow, reducing the effective wind speed. If the fixed-frame thrust force, which is a function of effective wind speed, is located in the half moving away from the flow, the thrust will be reduced. This translates to a reduction in applied yaw moment. A change in phase coupling between blade pitch input and yaw motion could therefore also lead to different behavior.

There exists no such reduction in tilt moment for the Helix method. A reduction of tilt moment would be expected if the platform undergoes either a surge or a platform pitch motion or a superposition of both. The fore-aft motion influences the relative velocity the turbine experiences, which affects the thrust of the turbine. However, the

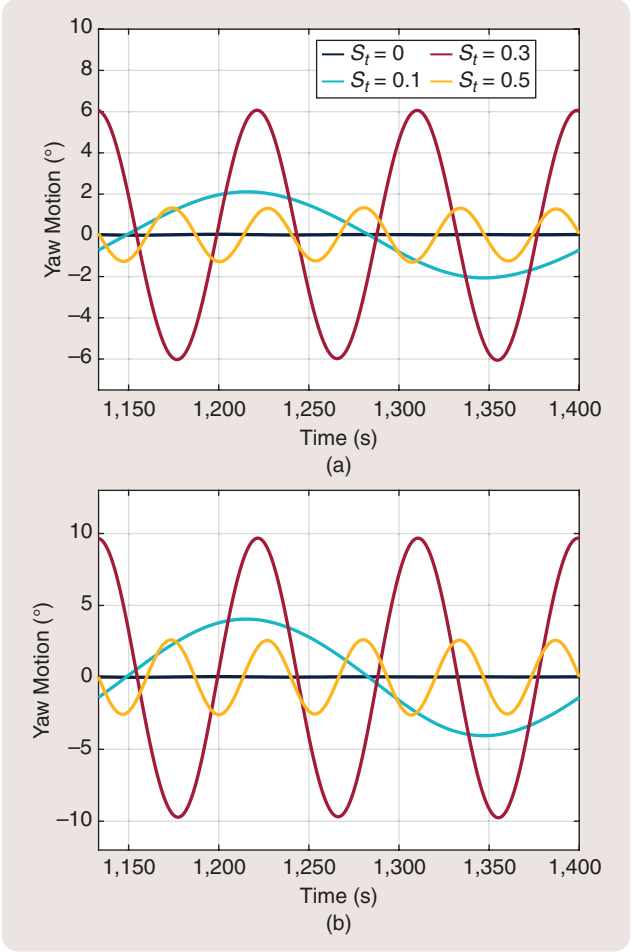

FIGURE 11 (a) The yaw motion for the 2° and (b) 4° Helix input amplitudes. The selected data are the results for the baseline cases and 3 different Strouhal numbers. The yaw motion at S_t = 0.30 exhibits the largest amplitude. The amplitude in yaw motion for the 2° input is slightly larger than the gain found in the frequency-response functions. (a). Amplitude 2°. (b) Amplitude 4°.

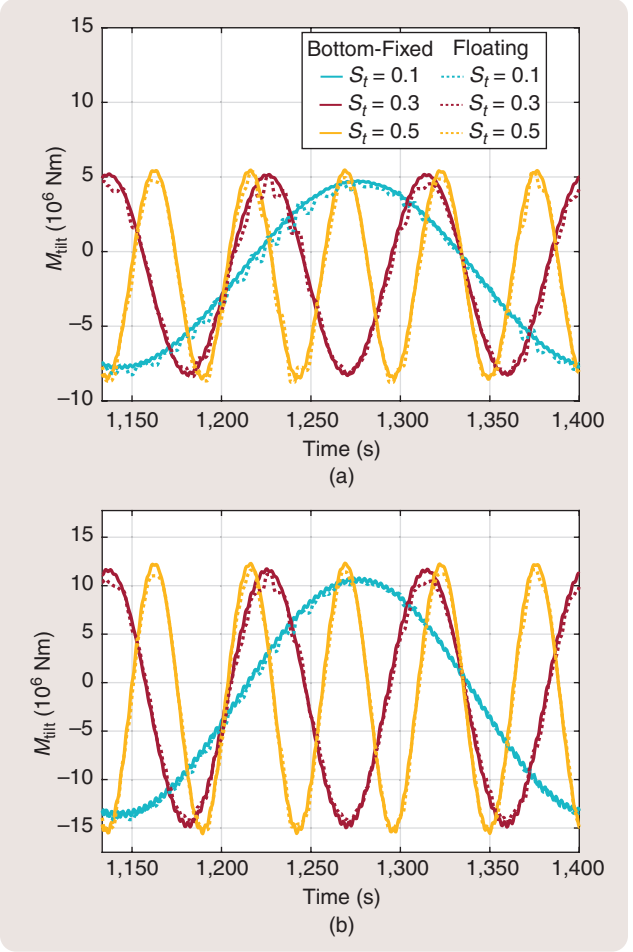

FIGURE 12 (a) The tilt moment for the 2° and (b) 4° blade pitch amplitudes for the same 3 Strouhal numbers considered in Figure 11. The solid lines represent the data from the bottom-fixed IEA 15-MW turbine and the dotted lines that of its floating counterpart. The high-frequency variations in tilt moment are due to the waves hitting the floating turbine. (a). Amplitude 2°. (b) Amplitude 4°.

eigenfrequencies in the surge and platform pitch are located at 0.007 and 0.036 Hz, respectively [63], the latter being outside the Strouhal range of interest. Both eigenfrequencies can be seen appearing in Figure 8.

For the effect on the Helix, these time-domain results can be interpreted as follows. Where for a bottom-fixed turbine, the thrust vector would move in a circular pattern over the rotor plane, it now resembles more of an oval path. As the wake mixing performance is related to the variation in the strength of the released vorticity, this reduction in yaw moment would, all other things being equal, lead to a reduction in wake mixing. However, this assumes that the extra yaw misalignment has no positive impact on this process, which is evaluated in the next section.

Average Wind Speed Results

An instantaneous snapshot of the wakes from both a top and side view is shown in Figures 14 and 15. Figures 14(a) and 15(a) show the wake of the bottom-fixed turbine, while Figures 14(b) and 15(b) show the wake of the floating turbine. For all actuated cases, the blade pitch amplitude is 4°. Areas of darker color indicate areas of low wind speed, and the higher the wind speed, the lighter the color. For the baseline cases ($S_t = 0.00$), wake recovery starts only around 5D. When the Helix is enabled, the wake shows patches of lower and higher wind speed. The patches of lower speed are part of the helical structure in the wake that is specific for the Helix method; see Figure 2. At higher frequencies, more of these patches appear as the thrust vector rotates with a higher velocity over the rotor plane, creating more helices. When comparing the wake for the bottom-fixed and floating turbines at $S_t = 0.30$, it can be seen that the wake for the floating turbine shows more lateral movement. Especially at 3D and 5D, the wake has moved farther sideways compared to the bottom-fixed turbine. In the side view, an upward deflection of the wake can be recognized. This deflection is a result of the platform pitch angle that results from the thrust force on the floating structure.

The wake mixing performance can be evaluated using the time-averaged downstream wind speed. The fact that the wake deflects under dynamic yaw motion is apparent from the snapshot depicted in Figure 14. Figure 16 shows the average gain in wind speed with respect to the baseline for both blade pitch amplitudes and turbines. Figure 16(a)/(c) shows the results for the bottom-fixed turbines, and Figure 16(b)/(d) presents the results for the floating turbine. For the 2° blade pitch amplitude cases, there is a distinct area where the gain in wind speed is highest. The largest increase, relative to the baseline, is achieved around $S_t = 0.3$ to $S_t = 0.4$ for the bottom-fixed turbine and around $S_t = 0.3$ to $S_t = 0.35$ for the floating turbine. The relative gain in windspeed is the same between both turbines; only the frequency range in which this gain can be achieved is smaller for the floating turbine. These data suggest that an optimal Strouhal number exists for wake mixing and that this remains the case for the floating turbine albeit for a smaller frequency range.

When the blade pitch amplitude is doubled, this area with the highest gain increases in size and moves farther upstream. This can be explained by the larger amplitude in the blade pitch angle, which increases the difference in magnitude of the shed vortices, accelerating the wake mixing process. Contrary to the 2° case, there is now a difference in relative gain between both turbines. Likewise, the area of the highest gain is smaller for the floating case. The downstream distance at which this gain is the highest remains similar between both turbines.

Wind speed is a measure of wake mixing, but recall that the goal is to maximize the power production of a wind farm. A large relative gain in wind speed might not equal a similar increase in power. The main cause for this is that the wind speed in the baseline case also increases as the wake recovers due to the natural mixing process. The relative contribution of the Helix might be lower farther downstream due to this, but the overall power of the wind farm could still

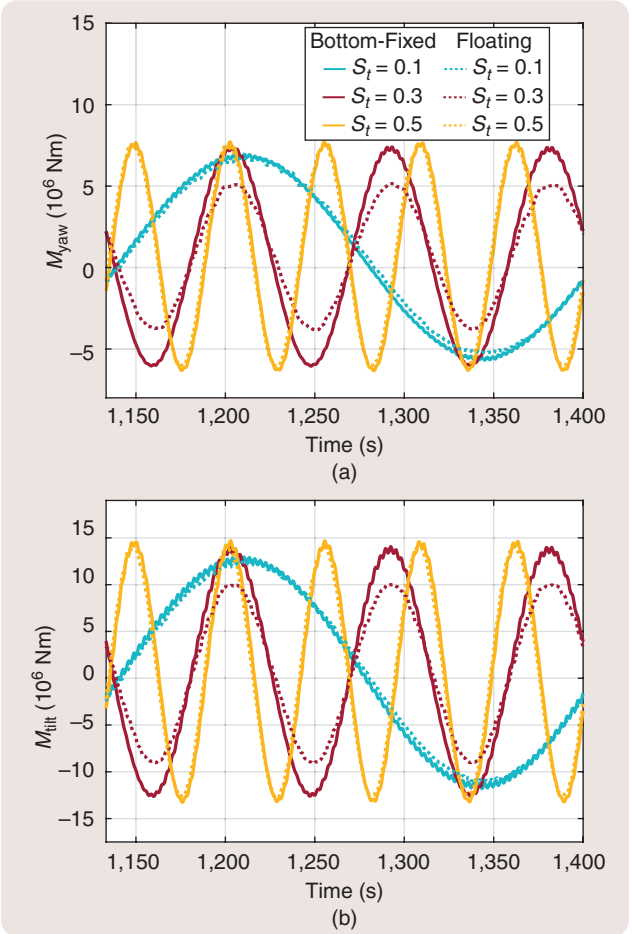

FIGURE 13 (a) The yaw moment for the 2° and 4° blade pitch amplitudes for the three different Strouhal numbers considered in Figure 11. The solid lines represent the data from the bottom-fixed IEA 15-MW turbine and the dotted lines that of its floating counterpart. For both $S_t = 0.10$ and $S_t = 0.5$, there is essentially no difference between bottom-fixed and floating cases. At the eigenfrequency in yaw motion, there is a notable decrease in the yaw moment. (a). Amplitude 2°. (b) Amplitude 4°.

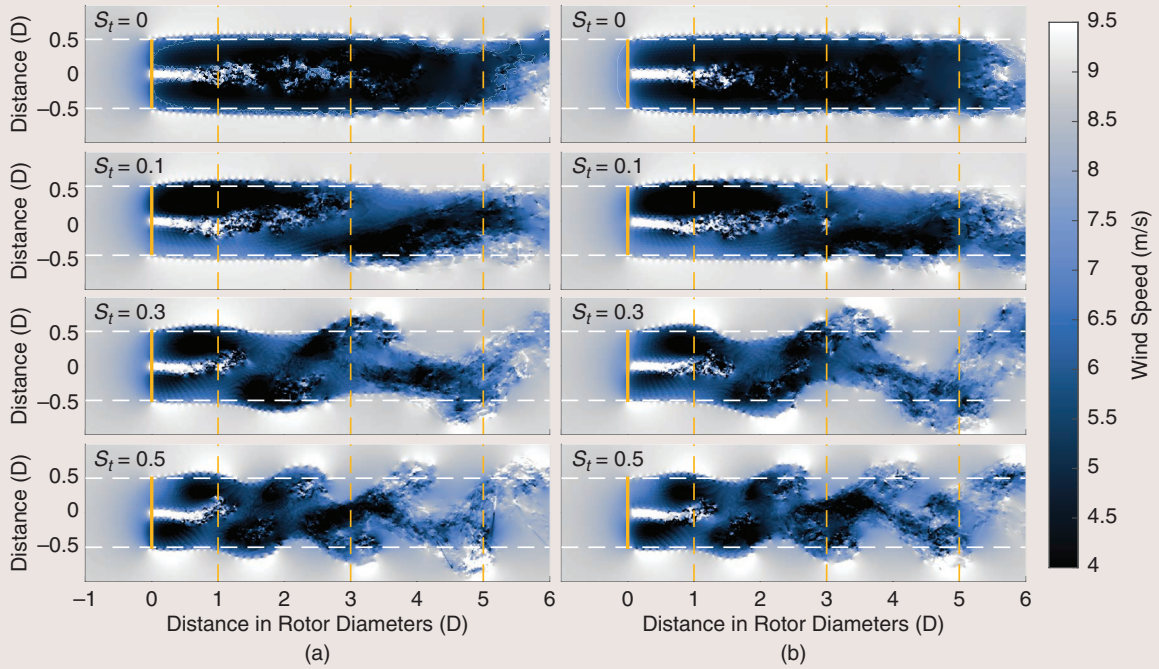

FIGURE 14 Instantaneous velocity slices at hub height for four different actuation frequencies. From top to bottom, the following frequencies are shown: $S_t = 0.00$, $S_t = 0.10$, $S_t = 0.30$ and $S_t = 0.50$. (a) Shows the results for the bottom-fixed turbine, and (b) shows the results for the floating turbine. The solid yellow line indicates the position of the turbine. Notice how the wake at $S_t = 0.30$ has deflected more at 3*D* and 5*D* for the floating turbine. (Source: Colors map courtesy of [80].)

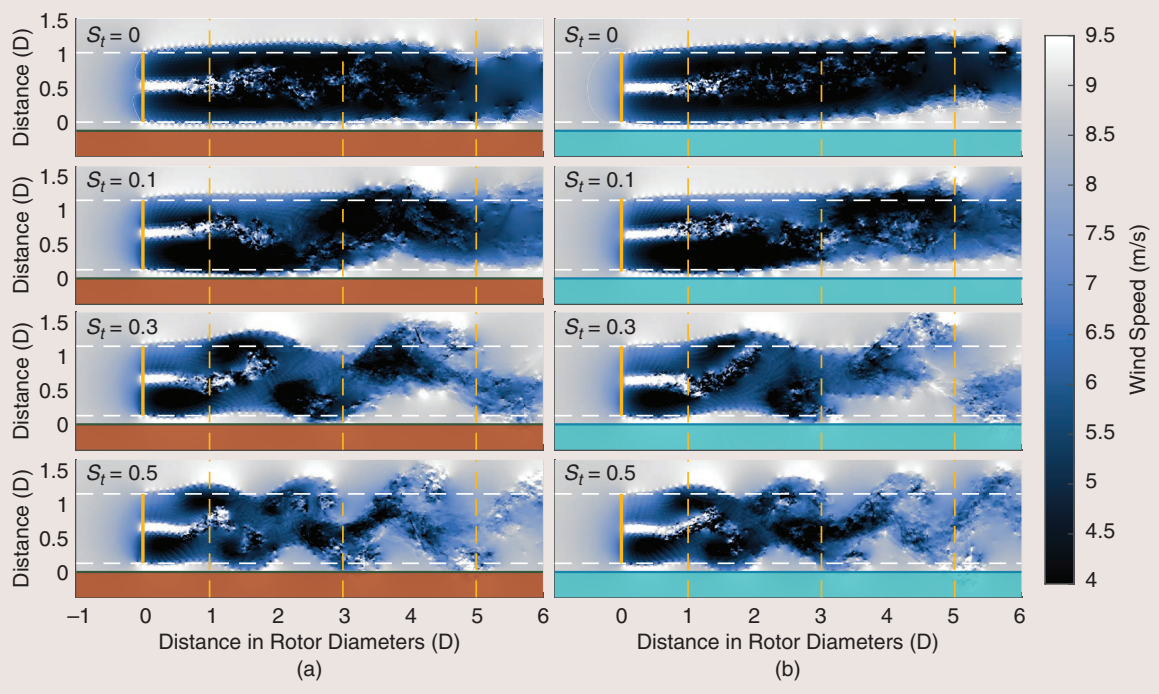

FIGURE 15 Instantaneous velocity slices taken from a side view for four different actuation frequencies. From top to bottom, the following frequencies are shown: $S_t = 0.00$, $S_t = 0.10$, $S_t = 0.30$ and $S_t = 0.50$. (a) Shows the results for the bottom-fixed turbine, and (b) shows the results for the floating turbine. The solid yellow line indicates the position of the turbine. The ground and sea are marked by the colored rectangles. Notice how even without actuation, the wake deflects upwards for the floating turbine, a result of the whole floating structure having a floater pitch offset. (Source: Color map courtesy of [80].)

be higher. How the results differ between wind speed and power production will be discussed in the next section.

Average Wind Farm Power Results

The power production of the wind farm is calculated by adding a second hypothetical IEA 15-MW turbine directly in line with the first turbine. The power production of this hypothetical turbine is calculated under the assumption that it is operating at a fixed power coefficient, using greedy control. With this assumption, the power can directly be calculated using the wind speed information from the previous section.

The power production of the upstream turbine is included in the analysis to calculate the power of the two-turbine farm. Actuating the Helix will result in a small loss in power for the upstream turbine, which is dependent on the blade pitching amplitude as well as its actuation frequency [57]. Likewise, yaw misalignment also causes a loss in power production. Because of these two effects, it is important to include the first turbine in the power calculation.

Figure 17 shows the average gain in wind farm power production with respect to the baseline case. The layout of the graph is the same as that of the wind data in Figure 16. Recall that this gain is still relative to the baseline case, that is, the highest gain doesn't necessarily equate to the largest possible power production within the presented dataset.

Looking at the data, the shape of the surfaces has changed significantly with respect to the wind speed data. In particular, the Strouhal range within which the highest gain can be achieved has narrowed to an area around $S_t = 0.3$ for the 2° case. Furthermore, the downstream distance at which it occurs is also one rotor diameter farther downstream, which is due to the wake continually recovering to higher wind speeds as it travels downstream. Similar to the wind speed results, the range in which the maximum is achieved for the floating turbine is smaller compared to the bottom-fixed case.

The 4° results show that the largest increase in power production relative to the baseline case is between 4*D* and 5D. The affected frequency range is still the same. For the floating

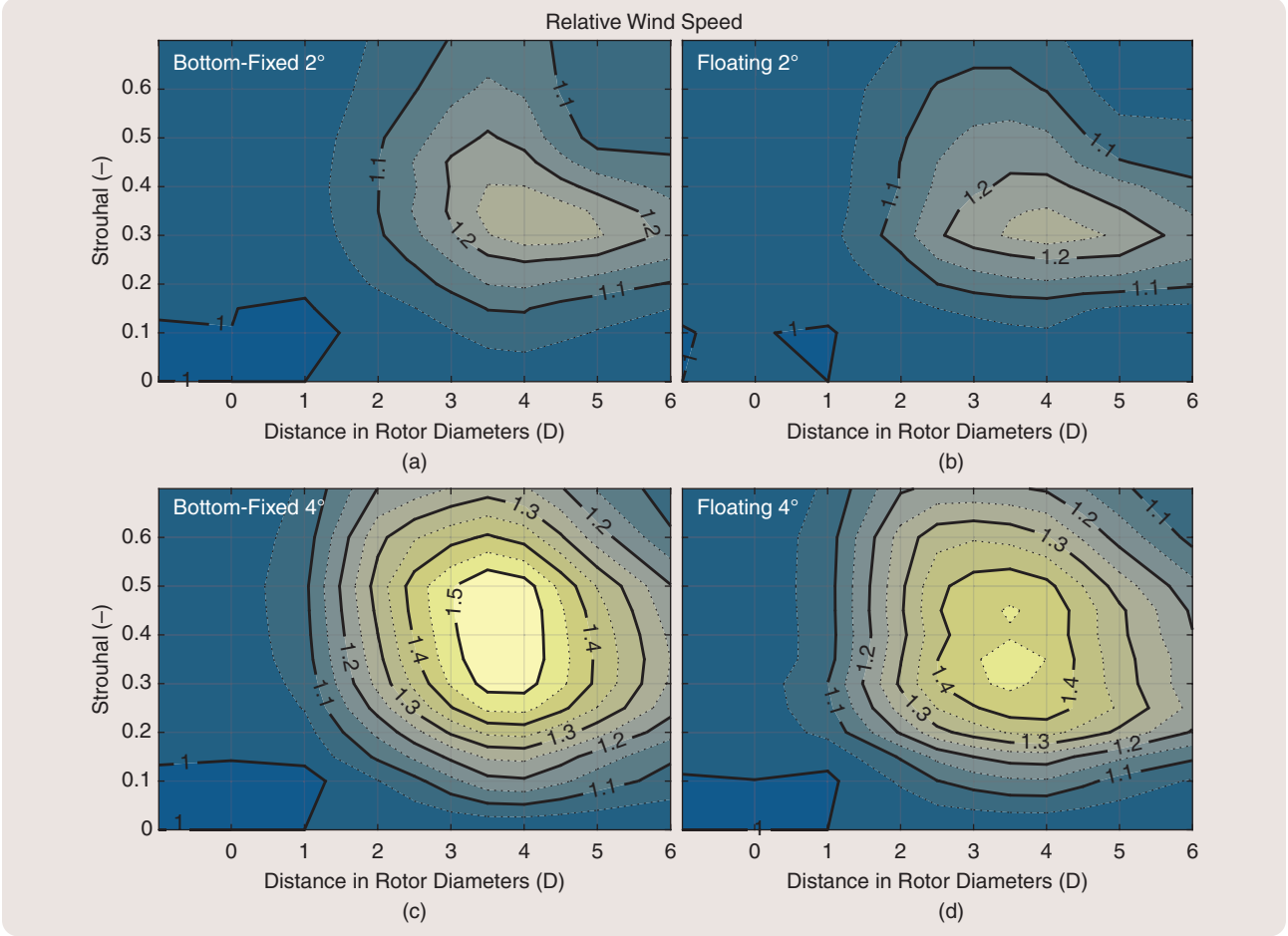

FIGURE 16 Contour plots showing the relative gain in the time-averaged downstream wind speed for both hypothetical bottom-fixed and floating turbines for both blade pitch amplitudes. The wind speed is measured directly behind the upstream turbine. For all actuated cases, wake recovery is accelerated with respect to the baseline case. Furthermore, there exists an area where the gain is highest, indicating that the relative wake recovery is highest at that Strouhal and distance. (a) Bottom-fixed 2°. (b) Floating 2°. (c) Bottom-fixed 4°. (d) Floating 4°. (Source: Color map courtesy of [80].)

turbine, this conclusion no longer holds for this input. While previously, there was one optimal frequency and distance, there are now two distinct areas for the floating turbine. These optima lie outside the range where this floating turbine has the largest yaw motion, indicating that the extra yaw motion cannot compensate for the loss in wake mixing.

Up to this point, all the results that have been presented are with respect to the baseline. Comparing the results to a baseline case shows how much can be gained from the Helix wake mixing technique for both bottom-fixed and floating turbines. Figure 18 shows the wind speed normalized with the inflow velocity. A gain of one would mean that the wake has fully recovered to the 9 m/s wind speed. The ideal mixing frequency can be identified to be around $S_t = 0.3$, which is in line with the results from the relative comparisons. The natural increase in wind speed for the baseline is also visible in the data.

When comparing the baseline case, represented by $S_t = 0.0$ for both floating and bottom-fixed turbines, the downstream distances at which the contour lines meet the x-axis are closer to $D = 0$ for the floating turbine than the bottom-fixed turbine. This implies that the floating baseline case has, on average, a higher wake recovery compared to the bottom-fixed turbine. Even without blade pitch actuation, the floating turbine is undergoing motions due to the waves hitting the floater, causing some degree of wake mixing. As such, when looking at absolute data, the floating turbine actually reaches a higher downstream velocity than the bottom-fixed case even though the relative gain is lower. In general, the absolute wind speeds echo the results of the relative wind speed results. The highest wind speeds are centered around $S_t = 0.30$, with the area extending down to $S_t = 0.20$ and up to $S_t = 0.40$. When the blade pitch angle is increased to 4°, the frequency and distance range increase in size.

FUTURE CHALLENGES

The overarching conclusion that can be drawn from the results presented in the previous two sections is that the interaction between the wake mixing controller and the floating turbine introduces additional challenges and opportunities.

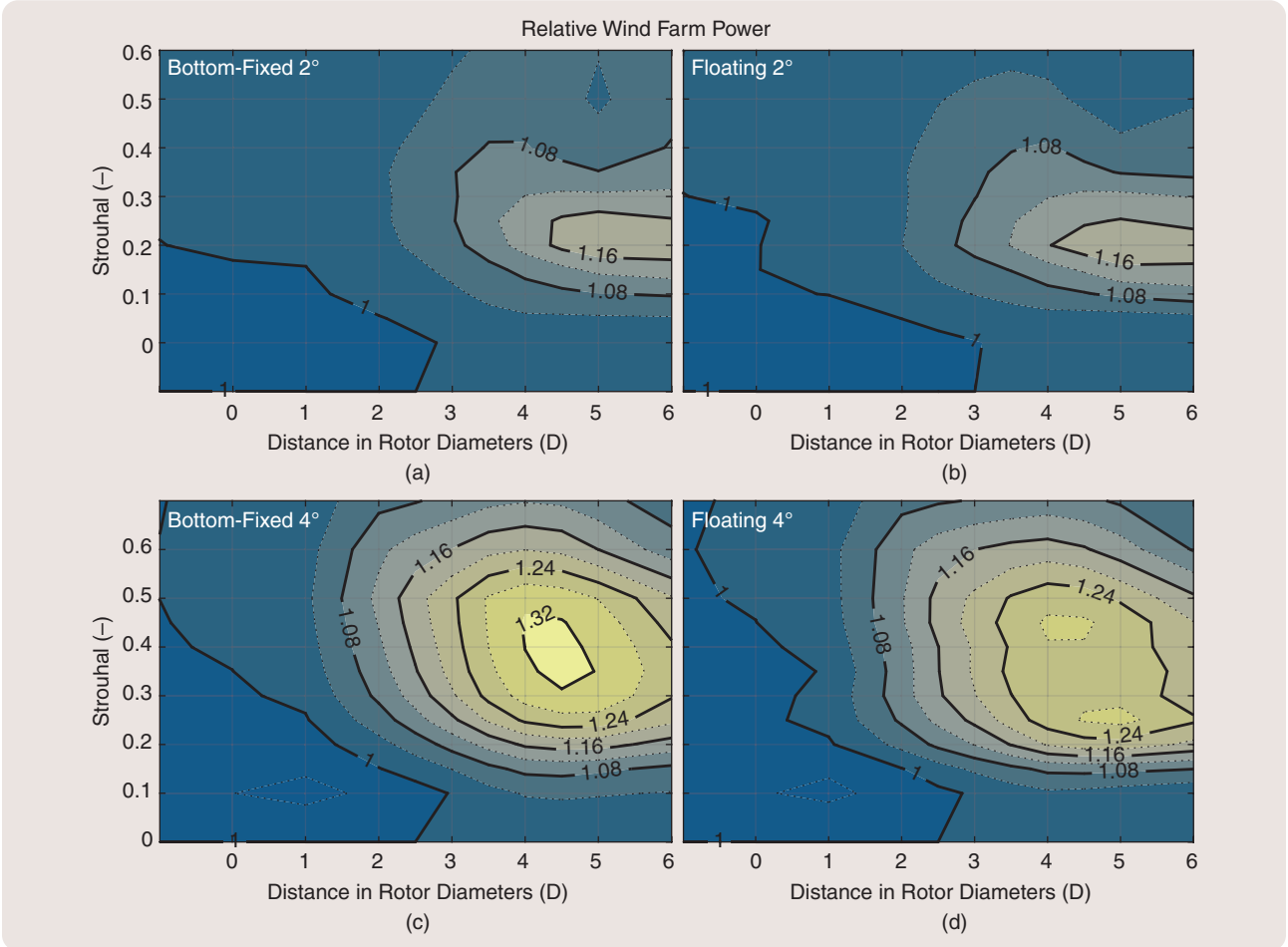

FIGURE 17 These contour plots show the relative gain in power production for both bottom-fixed and floating wind farms for both blade pitch blade amplitudes. As the wake recovers to higher windspeeds, more power can be produced by the wind farm. The areas of the highest relative gain have moved further downstream with respect to the wind speed results. For the 4° results with the floating turbine, two areas of equal gain appear. (a) Bottom-fixed 2°. (b) Floating 2°. (c) Bottom-fixed 4°. (d) Floating 4°. (Source: Color map courtesy of [80].)

These stem primarily from the additional six degrees of freedom that must be taken into account when designing a control system. Furthermore, the coupling between the controller and the floating turbine is dependent on the design of the floating turbine; see, for example, "Dynamics of the Pulse Wake Mixing Strategy." This work shows that the effectiveness of the Helix is impacted when coupled with the yawing degree of freedom of the floating turbine.

However, this work focused on only one type of turbine mounted on one floater design. In reality, more than 50 types of different floater designs are being considered in industry and academia alike [81]. All of these floaters have different dynamics depending on the type of floater, water depth in which it will be deployed, sea conditions, type of turbine, and many more parameters. The results discussed in this work could therefore be limited to this floater or this type of floater. This remains one of the main challenges that need to be considered when designing control solutions for a floating turbine.

For example, in [45], a similar investigation to the one presented in this work was executed for the Pulse wake mixing technique. In that work, the floating turbine considered was the National Renewable Energy Laboratory (NREL) 5-MW wind turbine [82] mounted on the OC3 platform [83], which is a single spar-type floater. For more details, see "Dynamics of the Pulse Wake Mixing Strategy." Its dominant motion was found to be the surge and platform pitch motion that, when combined, resulted in a fore-aft motion of the nacelle. Similar to this work, at the eigenfrequencies of that motion, the effectiveness of the wake mixing technique was reduced. Conducting the same experiments in that work on the floater used in this work would result in significantly different results because the surge and platform pitch motion of this floater is much smaller compared to the OC3. Likewise, conducting the experiments in this work on the OC3 and the antiresonance in M_{yaw} might not exist as the OC3 has no eigenfrequency in yaw motion.

This contrast is just one specific example of two different floating turbines with differing dynamics that both couple in a way that reduces the wake mixing technique. If the floater and turbine are designed independently of each other, these kinds of couplings have to be identified before

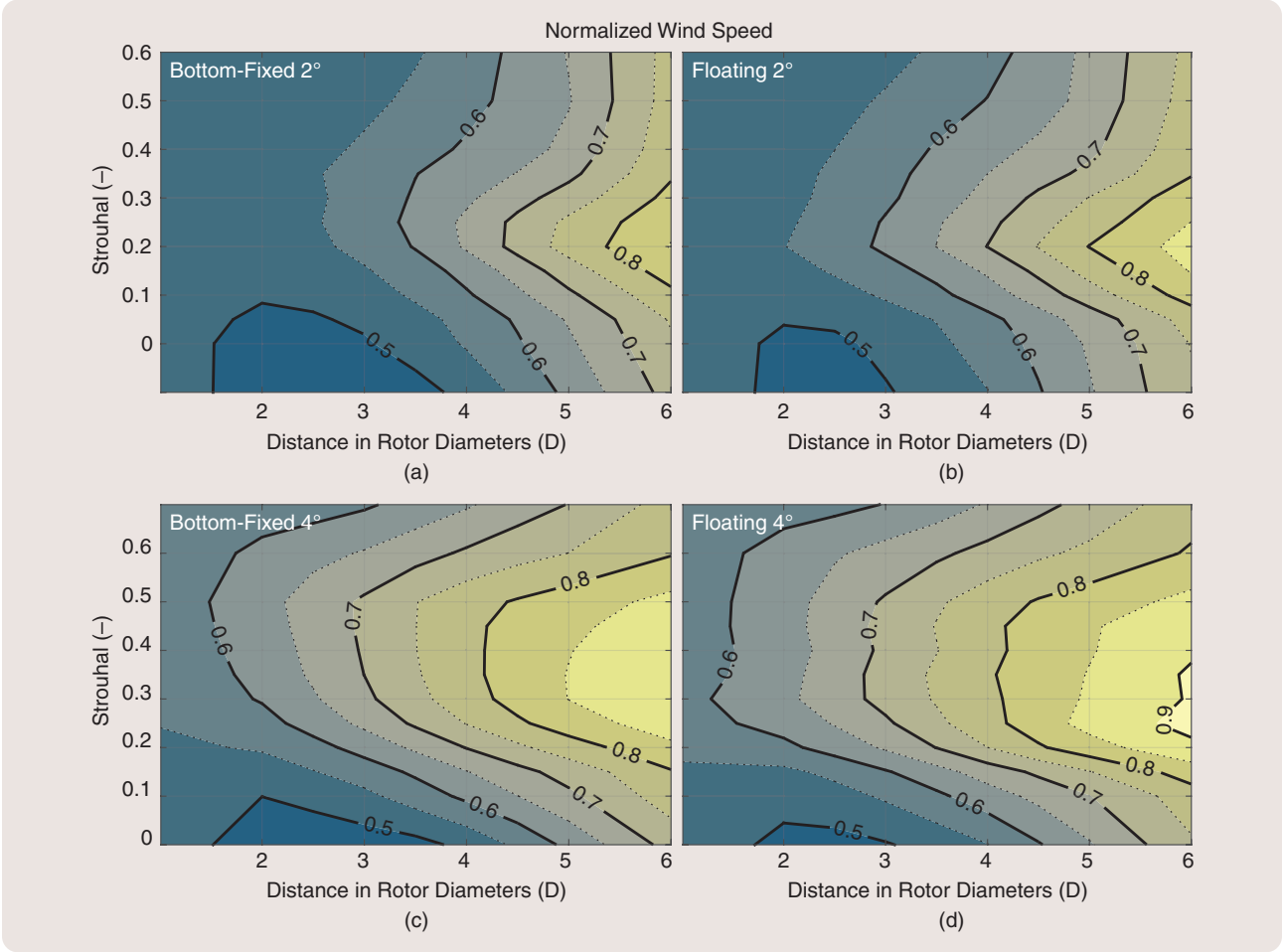

FIGURE 18 The absolute wind farm velocity normalized with $V_\infty = 9$ m/s. Between $S_t = 0.3$ and $S_t = 0.35$, the gain in wind speed is the highest for both types of turbines. Increasing the blade pitch amplitude increases the frequency range at which higher wind speeds can be achieved. (a) Bottom-fixed 2°. (b) Floating 2°. (c) Bottom-fixed 4°. (d) Floating 4°. (Source: Color map courtesy of [80].)

Dynamics of the Pulse Wake Mixing Strategy

The main content presented in this work focuses on the coupling between the Helix wake mixing method and the floating turbine. Throughout the work, a similar investigation for the Pulse wake mixing strategy [35] and a floating turbine is mentioned. This section will provide a short summary of the work executed in [45]. In that work, the floating turbine used is the NREL 5-MW wind turbine [82] mounted on the OC3 platform [83].

THE PULSE WAKE MIXING STRATEGY

The Pulse wake mixing strategy differs from the Helix method by the fact that it uses the collective blade pitch angle to disrupt the wake behind the turbine. Collectively pitching the blades creates a time-varying coefficient of the thrust of the turbine, which creates a time-varying wind field behind the turbine.

The optimal signal was derived in [33] and [35] using a gradient-based optimization process that optimized the thrust inputs for the turbines within a wind farm. The behavior of the optimized signal can be mimicked by the following signal:

$$C_t'(t) = 2 + A\sin\left(2\pi S_t \frac{V_\infty}{D} t\right) \tag{S1}$$

in which C_t' is the coefficient of thrust, A is the amplitude, and the other variables are as in (3a) and (4). For a turbine in greedy control, the Betz-optimal coefficient of thrust is $C_t' = 2$. Applying the signal in (S1) to a turbine results in it over- and underinducing around its optimal operating point. The signal in (S1) can be realized by setting a similar signal to the blade pitch angles of the turbine.

THE COUPLING BETWEEN THE PULSE AND TURBINE

When applying (S1) to a floating wind turbine, it will excite the surge and pitch motion. These two motions result in a motion of the nacelle. Depending on the phase difference between these two motions, they can either enhance or interfere with one another, as illustrated in Figure S9.

As the nacelle is moving backward and forward, the turbine will perceive a time-varying inflow velocity, which will create a time-varying thrust force not dissimilar to the one created when (S1) is applied to the turbine. To identify the coupling between the blade pitch input and resulting thrust force variation, an identification experiment is conducted. In this experiment, a chirp input is applied to the collective blade pitch angle. Based on this input and the measured thrust as output, the input–output spectra shown in Figure S10 are derived.

The results in Figure S10 indicate that there are two frequencies and one antiresonance for the nacelle displacement with this particular floating turbine. At the eigenfrequencies, there is a decrease in the peak-to-peak variation of the resulting thrust force, indicated by the antiresonances in the spectral data. When conducting time-domain simulations at the three frequencies that correspond to the two eigenfrequencies and the antiresonance in nacelle displacement, a reduction in thrust force as well as downstream wind speed is found, a result not dissimilar to the one presented in the main body of work.

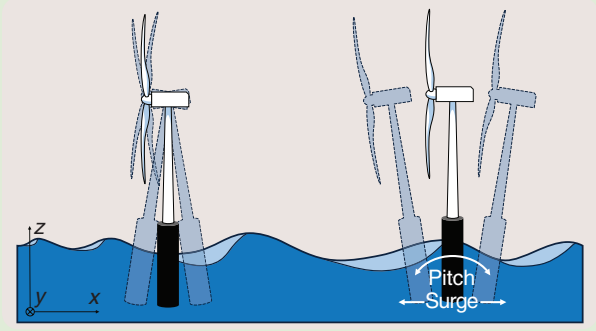

FIGURE S9 An example of how a similar platform pitch and surge motion can result in a different nacelle displacement.

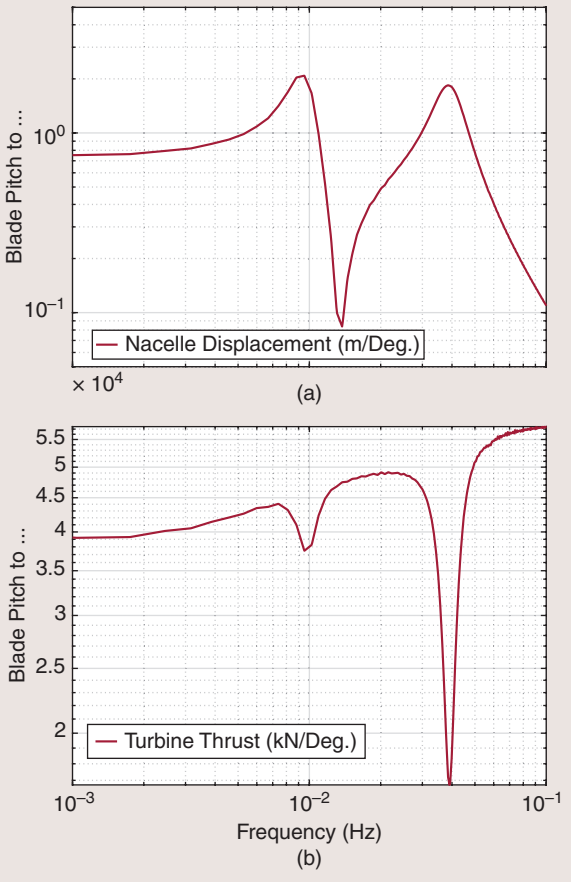

FIGURE S10 (a) and (b) The resulting spectra of the identification experiment for the Pulse wake mixing technique on the OC3 floating turbine. This turbine has two eigenfrequencies and one antiresonance in its nacelle displacement. At the eigenfrequencies, a reduction in the variation of thrust can be seen.

deciding on the type of wake mixing control that can be deployed. This can be solved by considering the control codesign of the floater, turbine, and its controls. This way, dual optima, such as in Figure 17, can be identified in the design stage, and the control dynamics can be optimized toward operating in that window.

CONCLUSION

Tackling the climate change challenge requires a significant increase in renewable energy capacity. This growth can be realized by increasing the efficiency of a wind farm by reducing the wake interaction between turbines. Control solutions designed for bottom-fixed turbines will have to be adapted to the floating turbines within those farms to accommodate the floating turbine dynamics. In this work, this transition is analyzed for the Helix method.

The effectiveness of the Helix wake mixing method depends on the application frequency and the blade pitch amplitude. For bottom-fixed turbines, this work shows that an ideal mixing frequency exists, between $S_t = 0.30$ and $S_t = 0.40$, which leads to the highest increase in wind speed downstream. A similar result was found for a floating turbine.

However, when the Helix is applied to a floating turbine, it will undergo a yaw motion. The magnitude of this motion is a function of the design of the floater and the actuation frequency of the Helix. For the turbine and floater used in this work, a frequency identification experiment showed that an eigenfrequency exists in yaw at $S_t = 0.30$. This yawing motion couples with the Helix method, and when yawing at the eigenfrequency, it leads to a reduction in yaw moment, captured as an antiresonance in the identification data. This reduction in yaw moment leads to a reduction in the effectiveness of the Helix as the difference in magnitude for the shed vortices is also lowered.

How this yaw motion and the reduction in yaw moment impact the overall effectiveness of the Helix is investigated using time-domain simulations. By evaluating the evolution of the downstream wind speed, a measure of the degree of wake mixing can be identified. At the 4° blade pitch amplitude used in this work, the relative gain is lower for the floating turbine compared to the bottom-fixed turbine. This is partly due to the higher baseline wind speed for the floating turbine, to which the results are compared, for the floating turbine and partly due to the yaw motion. The effect of the yaw motion can be better seen when looking at the relative power production of the two-turbine wind farm. It is interesting to see that rather than having one optimum, there are two for the floating turbine. These optima are centered around the yawing eigenfrequency, indicating that this coupling restricts the Helix.

The additional dynamics provide new challenges and opportunities in finding the right operating frequency for a wind farm operator desiring to use the Helix in a floating wind farm. Furthermore, future floater designs might introduce different dynamics to which wake mixing strategies couple, producing different results and requiring a new analysis. The latter can potentially be circumvented by incorporating wake mixing control into the design phase of the floating turbine. This way, it might be possible to design controls that enhance wake mixing through the codesign of their (hydro-)mechanical properties and controller.

ACKNOWLEDGMENT

This project is part of the Floatech project. The research presented in this article has received funding from the European Union's Horizon 2020 research and innovation program under Grant 101007142.

DATA AVAILABILITY

The data used in this work are available at the 4TU repository under the following DOI: 10.4121/617d13b8-a5aa-4f15-b8ca-a5c44a177f6e.v1 [84]. The data repository includes MATLAB scripts that, when run, produce the same figures as those presented in the article.

AUTHOR INFORMATION

Daniel van den Berg (d.g.vandenberg@tudelft.nl) received the M.Sc. degree in systems and control from the Delft University of Technology in 2020. Currently, he is a Ph.D. researcher in the group of Jan-Willem van Wingerden at the Delft Centre for Systems and Control, Delft, 2628 CN, The Netherlands. His research interests include wake mixing control for floating wind turbines.

Delphine De Tavernier received the Ph.D. degree in wind turbine aerodynamics from the Delft University of Technology. Currently, she is an assistant professor at the Flow Physics and Technology Department, Delft University of Technology, Delft, 2629 HS, The Netherlands. Her research interests include the unsteady aerodynamic behavior of (extremely) large wind turbines.

David Marten received the Ph.D. degree in physical engineering sciences from the Hermann-Föttinger Institute of the Technische Universität Berlin in 2019. Currently, he is a postdoctoral researcher at the Hermann-Föttinger Institute of the Technische Universität Berlin, 10623, Berlin, Germany. His research interests include aeroelasticity, hydrodynamics, and numerical optimizations. Since 2009, he has been actively involved in the ongoing advancement of the QBlade software as its main developer.

Joseph Saverin received the Dr.-Ing. degree in mechanical engineering from the Technische Universität Berlin. Currently, he is a postdoctoral researcher at the Hermann-Föttinger Institute of the Technische Universität Berlin, 10623, Berlin, Germany and head of the FLOATFARM project, a continuation of the FLOATECH project. His research interests include researching incompressible aerodynamics and hydrodynamics. He also works on the

development of efficient methods for aerodynamic and hydrodynamic simulation.

Jan-Willem van Wingerden received the M.Sc. and Ph.D. (both cum laude) degrees in mechanical engineering and control engineering from the Delft Center for Systems and Control, Delft University of Technology, Delft, The Netherlands, in 2004 and 2008, respectively. He is currently a full professor at the Delft University of Technology, Delft, 2628 CN, The Netherlands. His research interests include the development of data-driven controllers for wind turbines and wind farms. He is a Senior Member of IEEE.

REFERENCES

[1] "Information on the REPowerEU initiative." European Commission. Accessed: May 15, 2023. [Online]. Available: https://ec.europa.eu/info/strategy/priorities-2019-2024/european-green-deal/repowereu-affordable-secure-and-sustainable-energy-europe_en

[2] G. Costanzo, G. Brindley, and P. Cole. "Wind energy in Europe - 2022 statistics and the outlook for 2023-2027." Accessed: Jun. 02, 2023. [Online]. Available: https://windeurope.org/intelligence-platform/product/wind-energy-in-europe-2022-statistics-and-the-outlook-for-2023-2027/

[3] L. Ramirez. "Offshore wind in Europe - key trends and statistics 2022." Accessed: May 15, 2023. [Online]. Available: https://windeurope.org/intelligence-platform/product/offshore-wind-in-europe-key-trends-and-statistics-2022/

[4] "Offshore wind outlook 2019, distributed under the CC BY 4.0 license." IEA - International Energy Agency. Accessed: Jun. 15, 2023. [Online]. Available: https://www.iea.org/reports/offshore-wind-outlook-2019

[5] "Floating offshore wind vision statement." WindEurope. Accessed: May 15, 2023. [Online]. Available: https://windeurope.org/about-wind/reports/floating-vision-statement/

[6] P. Veers et al., "Grand challenges in the science of wind energy," *Science*, vol. 366, no. 6464, 2019, Art. no. eaau2027, doi: 10.1126/science.aau2027.

[7] R. J. Barthelmie et al., "Modelling and measuring flow and wind turbine wakes in large wind farms offshore," *Wind Energy*, vol. 12, no. 5, pp. 431–444, 2009, doi: 10.1002/we.348.

[8] R. J. Barthelmie et al., "Quantifying the impact of wind turbine wakes on power output at offshore wind farms," *J. Atmospheric Ocean. Technol.*, vol. 27, no. 8, pp. 1302–1317, 2010, doi: 10.1175/2010JTECHA1398.1.

[9] J. Meyers et al., "Wind farm flow control: Prospects and challenges," *Wind Energy Sci.*, vol. 7, no. 6, pp. 2271–2306, 2022, doi: 10.5194/wes-7-2271-2022.

[10] B. Clayton and P. Filby, "Measured effects of oblique flows and change in blade pitch angle on performance and wake development of model wind turbines," in *Proc. 4th BWEA Wind Energy Conf.*, Bedford, U.K.: BHRA Fluid Engineering, 1982, pp. 214–224.

[11] N. O. Jensen, *A Note on Wind Generator Interaction (Risø-M. 2411)*. Roskilde, Denmark: Risø National Laboratory, 1983.

[12] T. Göçmen, P. van der Laan, P.-E. Réthoré, A. P. Diaz, G. C. Larsen, and S. Ott, "Wind turbine wake models developed at the technical university of Denmark: A review," *Renewable Sustain. Energy Rev.*, vol. 60, pp. 752–769, Jul. 2016, doi: 10.1016/j.rser.2016.01.113.

[13] G. Mosetti, C. Poloni, and B. Diviacco, "Optimization of wind turbine positioning in large windfarms by means of a genetic algorithm," *Wind Eng. Ind. Aerodyn.*, vol. 51, no. 1, pp. 105–116, 1994, doi: 10.1016/0167-6105(94)90080-9.

[14] N. Kirchner-Bossi and F. Porté-Agel, "Realistic wind farm layout optimization through genetic algorithms using a Gaussian wake model," *Energies*, vol. 11, no. 12, 2018, Art. no. 3268, doi: 10.3390/en11123268.

[15] J. J. Thomas et al., "A comparison of eight optimization methods applied to a wind farm layout optimization problem," *Wind Energy Sci.*, vol. 8, no. 5, pp. 865–891, 2023, doi: 10.5194/wes-8-865-2023.

[16] A. P. J. Stanley, O. Roberts, J. King, and C. J. Bay, "Objective and algorithm considerations when optimizing the number and placement of turbines in a wind power plant," *Wind Energy Sci.*, vol. 6, no. 5, pp. 1143–1167, 2021, doi: 10.5194/wes-6-1143-2021.

[17] E. Quaeghebeur, R. Bos, and M. B. Zaaijer, "Wind farm layout optimization using pseudo-gradients," *Wind Energy Sci.*, vol. 6, no. 3, pp. 815–839, 2021, doi: 10.5194/wes-6-815-2021.

[18] R. Brogna, J. Feng, J. N. Sørensen, W. Z. Shen, and F. Porté-Agel, "A new wake model and comparison of eight algorithms for layout optimization of wind farms in complex terrain," *Appl. Energy*, vol. 259, Feb. 2020, Art. no. 114189, doi: 10.1016/j.apenergy.2019.114189.

[19] P. Parkin, R. Holm, and D. Medici, *The Application of PIV to the Wake of a Wind Turbine in Yaw*. Gottingen, Germany: Particle Image Velocimetry, 2001, pp. 155–162.

[20] D. Medici, "Experimental studies of wind turbine wakes: Power optimisation and meandering," Ph.D. dissertation, KTH Royal Institute of Technology, Stockholm, Sweden, 2005.

[21] "Siemens Gamesa now able to actively dictate wind flow at offshore wind locations." Siemens Gamesa Renewable Energy. Accessed: Jun. 02, 2023. [Online]. Available: https://www.siemensgamesa.com/en-int/newsroom/2019/11/191126-siemens-gamesa-wake-adapt-en

[22] A. Jiménez, A. Crespo, and E. Migoya, "Application of a LES technique to characterize the wake deflection of a wind turbine in yaw," *Wind Energy*, vol. 13, no. 6, pp. 559–572, 2010, doi: 10.1002/we.380.

[23] P. A. Fleming et al., "Evaluating techniques for redirecting turbine wakes using SOWFA," *Renewable Energy*, vol. 70, pp. 211–218, Oct. 2014, doi: 10.1016/j.renene.2014.02.015.

[24] M. Bastankhah and F. Porté-Agel, "Experimental and theoretical study of wind turbine wakes in yawed conditions," *J. Fluid Mech.*, vol. 806, pp. 506–541, Oct. 2016, doi: 10.1017/jfm.2016.595.

[25] P. M. O. Gebraad et al., "Wind plant power optimization through yaw control using a parametric model for wake effects—A CFD simulation study," *Wind Energy*, vol. 19, no. 1, pp. 95–114, 2016, doi: 10.1002/we.1822.

[26] P. Fleming et al., "Field test of wake steering at an offshore wind farm," *Wind Energy Sci.*, vol. 2, no. 1, pp. 229–239, 2017, doi: 10.5194/wes-2-229-2017.

[27] M. F. Howland, S. K. Lele, and J. O. Dabiri, "Wind farm power optimization through wake steering," *Proc. Nat. Acad. Sci.*, vol. 116, no. 29, pp. 14,495–14,500, 2019, doi: 10.1073/pnas.1903680116.

[28] P. M. Gebraad et al., "A data-driven model for wind plant power optimization by yaw control," in *Proc. Amer. Control Conf.*, Portland, OR, USA. Piscataway, NJ, USA: IEEE Press, 2014, pp. 3128–3134.

[29] P. A. Fleming, A. Ning, P. M. Gebraad, and K. Dykes, "Wind plant system engineering through optimization of layout and yaw control," *Wind Energy*, vol. 19, no. 2, pp. 329–344, 2016, doi: 10.1002/we.1836.

[30] A. P. J. Stanley, C. J. Bay, and P. Fleming, "Enabling control co-design of the next generation of wind plants," *Wind Energy Sci. Discuss.*, vol. 8, no. 8, pp. 1341–1350, 2023.

[31] M. Becker et al., "The revised FLORIDyn model: Implementation of heterogeneous flow and the Gaussian wake," *Wind Energy Sci.*, vol. 7, no. 6, pp. 2163–2179, 2022, doi: 10.5194/wes-7-2163-2022.

[32] M. J. van den Broek, D. De Tavernier, P. Hulsman, D. van der Hoek, B. Sanderse, and J. W. van Wingerden, "Free-vortex models for wind turbine wakes under yaw misalignment—A validation study on far-wake effects," *Wind Energy Sci.*, vol. 8, no. 12, pp. 1909–1925, 2023, doi: 10.5194/wes-8-1909-2023.

[33] J. Goit and J. Meyers, "Optimal control of energy extraction in wind-farm boundary layers," *J. Fluid Mech.*, vol. 768, pp. 5–50, Feb. 2015, doi: 10.1017/jfm.2015.70.

[34] C. H. Westergaard, "Method for improving large array wind park power performance through active wake manipulation reducing shadow effects," U.S. Patent 9,835,138, Dec. 2017.

[35] W. Munters and J. Meyers, "Towards practical dynamic induction control of wind farms: Analysis of optimally controlled wind-farm boundary layers and sinusoidal induction control of first-row turbines," *Wind Energy Sci.*, vol. 3, no. 1, pp. 409–425, 2018, doi: 10.5194/wes-3-409-2018.

[36] J. Frederik, B. Doekemeijer, S. Mulders, and J. W. van Wingerden, "On wind farm wake mixing strategies using dynamic individual pitch control," *J. Phys., Conf. Ser.*, vol. 1618, no. 2, 2020, Art. no. 22050.

[37] J. A. Frederik, B. M. Doekemeijer, S. P. Mulders, and J. W. van Wingerden, "The helix approach: Using dynamic individual pitch control to enhance wake mixing in wind farms," *Wind Energy*, vol. 23, no. 8, pp. 1739–1751, 2020, doi: 10.1002/we.2513.

[38] J. A. Frederik, B. M. Doekemeijer, and J. W. van Wingerden, "Enhanced wake mixing for floating wind turbines," U.S. Patent 20220412310A1, Nov. 2020.

[39] J. A. Frederik and J. W. van Wingerden, "On the load impact of dynamic wind farm wake mixing strategies," *Renewable Energy*, vol. 194, pp. 582–595, Jul. 2022, doi: 10.1016/j.renene.2022.05.110.

[40] A. A. W. van Vondelen, S. T. Navalkar, D. R. H. Kerssemakers, and J. W. van Wingerden, "Enhanced wake mixing in wind farms using the helix approach: A loads sensitivity study," in *Proc. Amer. Control Conf. (ACC)*, San Diego, CA, USA. Piscataway, NJ, USA: IEEE Press, 2023, pp. 831–836, doi: 10.23919/ACC55779.2023.10155965.

[41] S. F. Rodrigues, R. Teixeira Pinto, M. Soleimanzadeh, P. A. N. Bosman, and P. Bauer, "Wake losses optimization of offshore wind farms with moveable floating wind turbines," *Energy Convers. Manage.*, vol. 89, pp. 933–941, Jan. 2015, doi: 10.1016/j.enconman.2014.11.005.
[42] A. C. Kheirabadi and R. Nagamune, "Real-time relocation of floating offshore wind turbine platforms for wind farm efficiency maximization: An assessment of feasibility and steady-state potential," *Ocean Eng.*, vol. 208, Jul. 2020, Art. no. 107445, doi: 10.1016/j.oceaneng.2020.107445.
[43] T. Jard and R. Snaiki, "Real-time repositioning of floating wind turbines using model predictive control for position and power regulation," *Wind*, vol. 3, no. 2, pp. 131–150, 2023, doi: 10.3390/wind3020009.
[44] E. M. Nanos et al., "Vertical wake deflection for offshore floating wind turbines by differential ballast control," *J. Phys., Conf. Ser.*, vol. 1618, no. 2, 2020, Art. no. 022047, doi: 10.1088/1742-6596/1618/2/022047.
[45] D. van den Berg, D. De Tavernier, and J. W. van Wingerden, "The dynamic coupling between the pulse wake mixing strategy and floating wind turbines," *Wind Energy Sci.*, vol. 8, no. 5, pp. 849–864, 2023, doi: 10.5194/wes-8-849-2023.
[46] M. J. van den Broek, D. van den Berg, B. Sanderse, and J. W. van Wingerden, "Optimal control for wind turbine wake mixing on floating platforms," *IFAC-PapersOnLine*, vol. 56, no. 2, pp. 7656–7661, 2023, 22nd IFAC World Congress, doi: 10.1016/j.ifacol.2023.10.1165.
[47] D. van den Berg, D. D. Tavernier, and J. W. van Wingerden, "Using the Helix mixing approach on floating offshore wind turbines," *J. Phys., Conf. Ser.*, vol. 2265, 2022, Art. no. 042011.
[48] J. W. van Wingerden and D. G. van den Berg, "Enhanced wake mixing for floating wind turbines," Google Patents {W}O2022240292A1, Nov. 2022.
[49] D. Marten, "QBlade: A modern tool for the aeroelastic simulation of wind turbines," Ph.D. dissertation, Technische Universität Berlin, Berlin, Germany, 2020. [Online]. Available: 10.14279/depositonce-10646.
[50] E. A. Bossanyi, "Individual blade pitch control for load reduction," *Wind Energy*, vol. 6, no. 2, pp. 119–128, 2003, doi: 10.1002/we.76.
[51] E. A. Bossanyi, "Further load reductions with individual pitch control," *Wind Energy*, vol. 8, no. 4, pp. 481–485, 2005.
[52] S. P. Mulders, A. K. Pamososuryo, G. E. Disario, and J. W. van Wingerden, "Analysis and optimal individual pitch control decoupling by inclusion of an azimuth offset in the multiblade coordinate transformation," *Wind Energy*, vol. 22, no. 3, pp. 341–359, 2019, doi: 10.1002/we.2289.
[53] G. Bir, "Multi-blade coordinate transformation and its application to wind turbine analysis," in *Proc. 46th AIAA Aerospace Sci. Meeting Exhibit*, 2008, doi: 10.2514/6.2008-1300.
[54] D. van der Hoek, B. V. den Abbeele, C. S. Ferreira, and J. W. van Wingerden, "Maximizing wind farm power output with the helix approach: Experimental validation and wake analysis using tomographic particle image velocimetry," *Wind Energy*, vol. 27, no. 5, pp. 463–482, 2024.
[55] F. V. Mühle, F. M. Heckmeier, F. Campagnolo, and C. Breitsamter, "Wind tunnel investigations of an individual pitch control strategy for wind farm power optimization," *Wind Energy Sci. Discuss.*, vol. 9, no. 5, pp. 1–31, 2023.
[56] C. Muscari, P. Schito, A. Viré, A. Zasso, D. van der Hoek, and J. W. van Wingerden, "Physics informed DMD for periodic dynamic induction control of wind farms," *J. Phys., Conf. Ser.*, vol. 2265, no. 2, May 2022, Art. no. 022057, doi: 10.1088/1742-6596/2265/2/022057.
[57] E. Taschner, A. A. W. van Vondelen, R. Verzijlbergh, and J. W. van Wingerden, "On the performance of the Helix wind farm control approach in the conventionally neutral atmospheric boundary layer," *J. Phys., Conf. Ser.*, vol. 2505, no. 1, May 2023, Art. no. 012006, doi: 10.1088/1742-6596/2505/1/012006.
[58] H. Korb, H. Asmuth, and S. Ivanell, "The characteristics of helically deflected wind turbine wakes," *J. Fluid Mech.*, vol. 965, Jun. 2023, Art. no. A2, doi: 10.1017/jfm.2023.390.
[59] M. Coquelet, "Numerical investigation of wind turbine control schemes for load alleviation and wake effects mitigation," Ph.D. dissertation, UCL-Université Catholique de Louvain, 2022.
[60] J. Meyers and C. Meneveau, "Optimal turbine spacing in fully developed wind farm boundary layers," *Wind Energy*, vol. 15, no. 2, pp. 305–317, 2012, doi: 10.1002/we.469.
[61] R. J. Stevens, D. F. Gayme, and C. Meneveau, "Effects of turbine spacing on the power output of extended wind-farms," *Wind Energy*, vol. 19, no. 2, pp. 359–370, 2016, doi: 10.1002/we.1835.
[62] E. Gaertner et al. "IEA Wind TCP Task 37: Definition of the IEA 15-Megawatt Offshore Reference Wind Turbine." OSTI.GOV. Accessed: Aug. 08, 2024. [Online]. Available: https://www.osti.gov/biblio/1603478
[63] C. Allen et al., "Definition of the UMaine VolturnUS-S reference platform developed for the IEA wind 15-megawatt offshore reference wind turbine," National Renewable Energy Laboratory, Golden, CO, USA, 2020. [Online]. Available: https://www.osti.gov/biblio/1660012
[64] K. J. Astrom and R. M. Murray, *Feedback Systems: An Introduction for Scientists and Engineers*. Princeton, NJ, USA: Princeton Univ. Press, 2008.
[65] J. G. Leishman, M. J. Bhagwat, and A. Bagai, "Free-vortex filament methods for the analysis of helicopter rotor wakes," *J. Aircraft*, vol. 39, no. 5, pp. 759–775, 2002, doi: 10.2514/2.3022.
[66] J. G. Leishman, M. J. Bhagwat, and S. Ananthan, "The vortex ring state as a spatially and temporally developing wake instability," *J. Amer. Helicopter Soc.*, vol. 49, no. 2, pp. 160–175, 2004, doi: 10.4050/JAHS.49.160.
[67] K. Shaler, E. Branlard, A. Platt, and J. Jonkman, "Preliminary introduction of a free vortex wake method into OpenFAST," *J. Phys., Conf. Ser.*, vol. 1452, no. 1, 2020, Art. no. 012064, doi: 10.1088/1742-6596/1452/1/012064.
[68] D. Marten, M. Lennie, G. Pechlivanoglou, C. N. Nayeri, and C. O. Paschereit, "Implementation, optimization, and validation of a nonlinear lifting line-free vortex wake module within the wind turbine simulation code QBLADE," *J. Eng. Gas Turbines Power*, vol. 138, no. 7, 2016, Art. no. 072601, doi: 10.1115/1.4031872.
[69] M. Jeon, S. Lee, T. Kim, and S. Lee, "Wake influence on dynamic load characteristics of offshore floating wind turbines," *AIAA J.*, vol. 54, no. 11, pp. 3535–3545, 2016, doi: 10.2514/1.J054584.
[70] C. R. Shapiro, D. F. Gayme, and C. Meneveau, "Modelling yawed wind turbine wakes: A lifting line approach," *J. Fluid Mech.*, vol. 841, Feb. 2018, Art. no. R1, doi: 10.1017/jfm.2018.75.
[71] S. N. Rodriguez, J. W. Jaworski, and J. G. Michopoulos, "Stability of helical vortex structures shed from flexible rotors," *J. Fluids Struct.*, vol. 104, Jul. 2021, Art. no. 103279, doi: 10.1016/j.jfluidstructs.2021.103279.
[72] D. Marten et al., "Predicting wind turbine wake breakdown using a free vortex wake code," *AIAA J.*, vol. 58, no. 11, pp. 4672–4685, 2020, doi: 10.2514/1.J058308.
[73] M. Abdullah, A. Yatim, C. Tan, and R. Saidur, "A review of maximum power point tracking algorithms for wind energy systems," *Renewable Sustain. Energy Rev.*, vol. 16, no. 5, pp. 3220–3227, 2012, doi: 10.1016/j.rser.2012.02.016.
[74] I. R. Young, *Wind Generated Ocean Waves*. Amsterdam, The Netherlands: Elsevier, 1999.
[75] *Wind Energy Generation Systems - Part 3-1: Design Requirements for Fixed Offshore Wind Turbines*, IEC Standard 61400-3-1:2019, International Electrotechnical Commission, Geneva, Switzerland, Apr. 2019.
[76] K. Hasselmann et al., "Measurements of wind-wave growth and swell decay during the Joint North Sea Wave Project (JONSWAP)," *Ergaenzungsheft Zur Deutschen Hydrographischen Zeitschrift, Reihe A*, Jan. 1973, pp. 1–95.
[77] J. M. J. Journée, W. W. Massie, and R. H. M. Huijsmans. "Offshore hydromechanics, 3rd ed." TU Delft OpenCourseWare. Accessed: May 15, 2023. [Online]. Available: https://ocw.tudelft.nl/courses/offshore-hydromechanics
[78] L. Brandetti and D. van den Berg. "QBlade 2.0.5.2 matlab tutorial." TU Delft Research Portal. Accessed: Aug. 08, 2024. [Online]. Available: https://research.tudelft.nl/en/datasets/qblade-2052-matlab-tutorial
[79] E. A. Bossanyi, "The design of closed loop controllers for wind turbines," *Wind Energy*, vol. 3, no. 3, pp. 149–163, 2000, doi: 10.1002/we.34.abs.
[80] F. Crameri, G. E. Shephard, and P. J. Heron, "The misuse of colour in science communication," *Nature Commun.*, vol. 11, no. 1, 2020, Art. no. 5444, doi: 10.1038/s41467-020-19160-7.
[81] "Floating wind foundations: Out of more than 50, which concepts will dominate the market?" Aegir. Insights. Accessed: Jul. 4, 2023. [Online]. Available: https://www.aegirinsights.com/floating-wind-foundations-out-of-more-than-50-which-concepts-will-dominate-the-market
[82] J. Jonkman, S. Butterfield, W. Musial, and G. Scott, "Definition of a 5-MW reference wind turbine for offshore system development," National Renewable Energy Lab. (NREL), Golden, CO, USA, Tech. Rep. NREL/TP-500-38060; TRN: US200906%%69, 2009.
[83] J. Jonkman, "Definition of the floating system for phase IV of OC3," National Renewable Energy Lab. (NREL), Golden, CO, USA, Tech. Rep. NREL/TP-500-47535; TRN: US201010%%826, 2010.
[84] D. van den Berg. "Frequency and time response data presented in: Wake mixing control for floating wind farms (Published in the Control Systems Magazine)." 4TU.ResearchData. Accessed: Aug. 08, 2024. [Online]. Available: https://data.4tu.nl/datasets/617d13b8-a5aa-4f15-b8ca-a5c44a177f6e/1
[85] Y. Niu, A. Dwivedi, J. Sathiaraj, P. P. Lathi, and R. Nagamune, "Floating offshore wind farm control via turbine repositioning: Unlocking the potential unique to floating offshore wind," *IEEE Control Syst.*, vol. 44, no. 5, pp. 106–129, Oct. 2024.